© 2022. Published by The Company of Biologists Ltd | Journal of Experimental Biology (2022) 225, jeb242872. doi:10.1242/jeb.242872

RESEARCH ARTICLE

Flight activity and age cause wing damage in house flies

Henja-Niniane Wehmann*, Thomas Engels and Fritz-Olaf Lehmann‡

ABSTRACT

Wing damage attenuates aerial performance in many flying animals such as birds, bats and insects. Insect wings are especially light in order to reduce inertial power requirements for flight at elevated wing flapping frequencies. There is a continuing debate on the factors causing wing damage in insects, including collisions with objects, mechanical stress during flight activity, and aging. This experimental study addressed the reasons for and significance of wing damage for flight in the house fly *Musca domestica*. We determined natural wing area loss under two housing conditions and recorded flight activity and flight ability throughout the animals' lifetime. Our data show that in animals with eventually pronounced damage, wing damage occurs on average after 6 h of flight, is sex specific and depends on housing conditions. Statistical tests show that physiological age and flight activity have similar significance as predictors for wing damage. Tests on freely flying flies showed that minimum wing area for active flight is approximately 10–34% below the initial area and requires a left–right wing area asymmetry of less than approximately 25%. Our findings broadly confirm predictions from simple aerodynamic theory based on mean wing velocity and area, and are also consistent with previous wing damage measurements in other insect species.

KEY WORDS: Insect flight, Loss of wing area, Locomotor capacity, *Musca domestica*

INTRODUCTION

Insect wings are delicate structures which often break over the course of an animal's lifetime. Multiple reasons for wing damage have been proposed, including interactions between conspecifics during sexual competition and mating (Alcock, 1996; Burkhard et al., 2002; Pinheiro, 1990; Ragland and Sohal, 1973), injuries during oviposition, building and defending a nest, and intraspecific and interspecific aggression, competition and predation (Benson, 1972; Nalepa, 2012; O'Neill et al., 2015; Rajabi et al., 2020). Besides the above reasons, wing damage predominantly results from the collision of wings with objects (Burkhard et al., 2002; Foster and Cartar, 2011; Rhainds and Brodersen, 2012) and thus increases with increasing flight activity (Hayes et al., 1998). In general, adverse habitats (Lee et al., 2006) and high population densities of animals in captivity favour wing damage (Ragland and Sohal, 1973). Wing damage also depends on the sex ratio within an insect group (Rhainds and Brodersen, 2012) and is sex specific (Burkhard et al., 2002; Kiritani et al., 2013; Lee et al., 2006; Mueller and Wolf-Mueller, 1993; Ragland and Sohal, 1973; Rhainds and Brodersen, 2012). The relevance of wing damage for the fitness of flying insects is due to the negligible healing capacity of broken wings, although puzzling findings previously suggested that wings may regrow after complete extirpation (Kammerer, 1907; Werber, 1907, 1911). These findings, however, were also explained by the deformation of dead cuticle material and not a regeneration of living tissue (Křiženecký, 1914). Wing damage in holometabolic animals thus accumulates over the animal's lifetime and is used for estimations of chronological (Allsopp, 1985; Hargrove, 2020; Mueller and Wolf-Mueller, 1993) and physiological age (Burkhard et al., 2002; Hayes et al., 1998).

There is ongoing controversy on the development of wing damage in insects and its dependency on flight activity. Several authors reported an increasing rate of wing damage with increasing lifetime (Foster and Cartar, 2011; Higginson and Barnard, 2004), while others found the opposite (Mueller and Wolf-Mueller, 1993; O'Neill et al., 2015). For example, Mountcastle and Combes (2014) proposed that insect wings with broken tips accrue less additional damage. They argued that frayed and shorter wings are more compliant than intact wings when hitting a solid object and thus the rate of wing wear should decrease with increasing lifetime. Studies on 'lifetime potential' concepts, for example in bumblebees, suggest that flight with damaged wings leads to faster physiological senescence and premature death (Cartar, 1992). Vance (2009) observed an inability of older animals to compensate for wing area loss by an appropriate increase in wing flapping frequency, which implies a loss of fitness. There are experimental findings on male flies that supposedly showed a reduction in longevity when the wings were artificially removed from the body. This result has been attributed to an overuse of leg motion as a result of mating attempts because it was not present in solitary males (Ragland and Sohal, 1973).

The behavioural and fitness consequences of wing area loss for flight are manifold and the animals' compensatory mechanisms remarkable. For example, (i) bumblebees with damaged wings often have unchanged flight behaviours compared with intact conspecifics (Haas and Cartar, 2008), (ii) dragonflies with a missing hindwing are still able to turn, land on a moving object and catch flies, with little difference in locomotor force production compared with intact animals (Kassner et al., 2016), and (iii) butterflies with wing damage still defend territories against intruders with intact wings (Monge-Nájera et al., 1998). The last, however, may be explained by the highly ritualised nature of butterfly fights, in which the intruder usually loses (Davies, 1978). Nevertheless, the loss of wing area typically attenuates flight capacity. Insects with damaged wings fly more slowly than those with intact wings (Combes et al., 2010; Fischer and Kutsch, 2000; Haas and Cartar, 2008; Jantzen and Eisner, 2008; Muijres et al., 2017) and maximum acceleration and manoeuvrability are usually reduced (Combes et al., 2010; Haas and Cartar, 2008; Mountcastle et al., 2016). It has been suggested that this reduction increases the risk of predation (Cartar, 1992; Combes et al., 2010; Dukas and Dukas, 2011; Jantzen and Eisner, 2008; Vance and Roberts, 2014) and social insects such as bees may suffer from reduced performance of wing-damaged foragers (Dukas and Dukas, 2011; Higginson and

Department of Animal Physiology, University of Rostock, 18059 Rostock, Germany. *Present address: Institute of Semiconductor Technology, Technische Universität Braunschweig, 38106 Braunschweig, Germany.

‡Author for correspondence (fritz.lehmann@uni-rostock.de)

F.-O.L., 0000-0002-9511-3651

Received 17 May 2021; Accepted 1 December 2021

Journal of Experimental Biology (2022) 225, jeb242872. doi:10.1242/jeb.242872

Barnard, 2004; Johnson and Cartar, 2014). Similar results have been reported for small solitary carpenter bees (Rehan and Richards, 2010). In general, wing damage reduces the animal's load-lifting capacity, although neither the shape nor the symmetry of damage seems to be significant (Buchwald and Dudley, 2010; Fernández et al., 2017; Roberts and Cartar, 2015). Data show that insects lose their flight ability if wing area loss exceeds ∼33–40% of the initial area (Haas and Cartar, 2008; Ragland and Sohal, 1973). Some four-winged insects may still actively fly with only two wings, i.e. a ∼50% reduction in total wing area (Kassner et al., 2016), and butterflies without hindwings produce enough lift for flight but at the cost of lower flight and turning speeds (Jantzen and Eisner, 2008).

To compensate for the loss of wing area, many insects such as moths, bumblebees and dragonflies adapt their wing kinematics to the smaller lift-generating surface, increasing or decreasing wingbeat frequency (Danzer, 1956; Fernández et al., 2012, 2017; Hargrove, 1975; Hedenström et al., 2001; Jantzen and Eisner, 2008; Kassner et al., 2016; Kingsolver, 1999; Muijres et al., 2017; Roberts and Cartar, 2015; Sotavalta, 1952a; Vance and Roberts, 2014) and increasing wingbeat amplitude (Buchwald and Dudley, 2010; Fernández et al., 2017; Johnson and Cartar, 2014; Lyu et al., 2020; Muijres et al., 2017; Vance and Roberts, 2014). While in Diptera the changes in wing beat frequency are thought to result from the reduction in mass load on the mechanical thoracic oscillator (Sotavalta, 1952b), the changes in wingbeat frequency of insects with synchronous flight muscles necessarily result from neural adjustments in muscle contraction (e.g. Wilson and Weis-Fogh, 1962). Besides wingbeat frequency and amplitude, insects also change their wing tip path during upstroke and downstroke and body posture in response to wing wear (Fernández et al., 2012; Lyu et al., 2020; Muijres et al., 2017) that moreover alter aerodynamic force production and moment control around yaw, pitch and roll axes of the insect body.

To investigate the dependency of wing damage on both flight activity and age in an insect, and to estimate the significance of wing area loss for flight capacity, this study experimentally investigated the time evolution and behavioural impact of wing damage in the house fly *Musca domestica*. We scored flight activity throughout the entire lifetime of adult animals, mapped their wing wear at regular intervals and tested the ability of animals with damaged wings to support their body weight in free flight. The statistical analyses suggest that wing area loss in flies follows a logistic function and depends equally on flight activity and age. We also found that the animal's active flight capacity ceases when ∼10–34% of total wing area is lost.

MATERIALS AND METHODS

This study encompasses two experimental approaches: first, an assay with which we determined the progression of wing wear and flight activity in small groups of flies kept in small transparent cylindrical plastic containers (height, 72 mm; diameter, 48 mm; Fig. 1C) with ∼130 cm^3 volume (container experiment); and second, a behavioural assay, in which we scored wing wear and the flies' ability to freely fly (free-flight experiment) in a ∼2000 times larger mesh flight cage (52×52×93 cm^3, ∼0.25 m^3 volume). Both approaches comprised lifetime measurements (container experiment, total experimental time: 153 days; free-flight experiment, total experimental time: 94 days). If not stated otherwise, all data are given as means±s.d. Data are available through Dryad (Lehmann, 2021).

Animals

In all experiments, we used house flies *Musca domestica* L. from a laboratory strain obtained from the German Federal Environmental Agency (Fig. 1A,B). The flies were kept under a 12 h:12 h light:dark cycle and supplied *ad libitum* with sugar, powdered milk and water; females had the opportunity for oviposition on a moist medium. Larvae were reared in separate plastic containers, and transferred into plastic tubes after pupation, in which the adults hatched. For experiments, all animals were marked with small amounts of paint on their thorax (Pelikan, Hannover, Germany).

For container experiments, the animals were sorted according to sex, and moved from their hatching container into the experimental container at a median age of 0.5 days, where they were kept until they died. There was no significant difference in transfer age between males and females (Welch two-sample *t*-test, P=0.39). We estimated body mass when the flies were ∼4.5 days old. Dead flies were replaced by flies of the same age from a control container in order to keep group sizes constant in the experimental containers (see below). We did not collect wing damage data from flies that had been added as a replacement. In total, we tested 72 flies in 18 groups (4 flies per container) and the final number analysed was 27 females and 36 males. Body mass was ∼18.6±2.8 mg in females and ∼14.1±2.4 mg in males (Fig. 2A). Females were significantly heavier than males (Welch two-sample *t*-test, P<0.001). Wing area was also greater in females than in males (Fig. 2B,E) in both experimental approaches, and significantly increased with increasing body mass (Fig. 2C). For free-flight experiments, we placed 10 females and 10 males immediately after hatching into the mesh cage and kept them there until they died. As three flies were accidentally killed during the experimental period, the data in this approach stem from 8 females and 9 males. In this case, dead flies were not replaced.

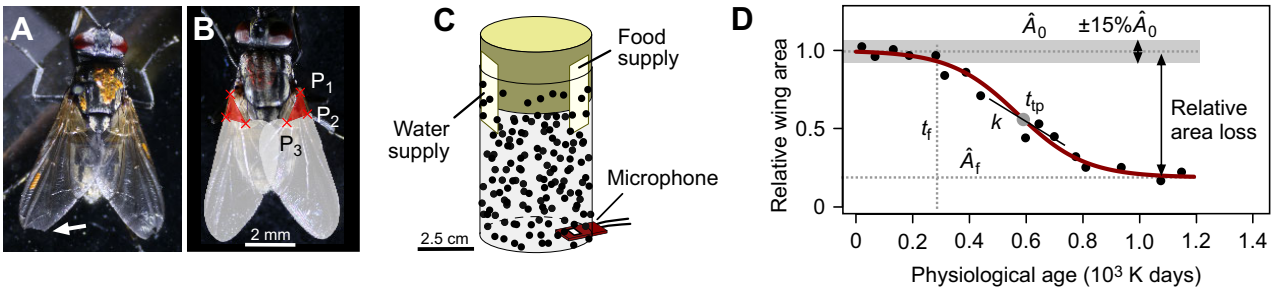

Fig. 1. Methods and mathematical procedure. (A) A female house fly, marked by orange paint on the thorax; the arrow points to a local loss of wing membrane at the wing tip. (B) Traced wing masks (white) for area estimations and red area (P_1–P_3), which indicates the hinge area and position for wing alignment. (C) Transparent fly container for flight activity measurements with surrounding random dot pattern for visual guidance. A microphone is mounted in a hole at the bottom and paper strips provide water and food. (D) Parameters of the logistic fit model as used for estimations of wing damage development. $\hat{A}_0$, normalised initial wing area; $\hat{A}_f$, normalised wing area at death; k, logistic growth rate of the fitted function (not visible; related to slope at the inflexion point, see Eqn 7); t_f, beginning of wing damage at 0.85$\hat{A}_0$; and t_{tp}, time coordinate of inflexion point of the fitted function. Physiological age is in Kelvin days (K days).

Journal of Experimental Biology

Journal of Experimental Biology (2022) 225, jeb242872. doi:10.1242/jeb.242872

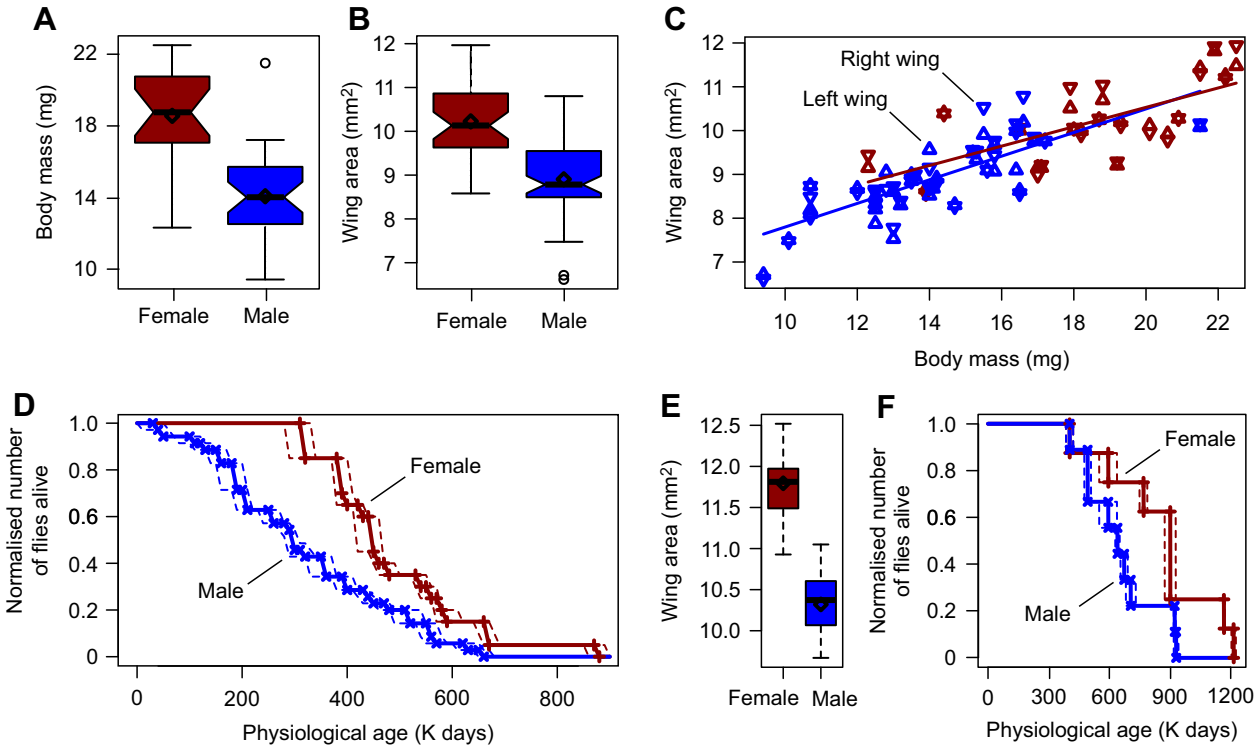

Fig. 2. Body mass, initial wing area and survival rate of flies. Initial (A) body mass and (B) wing area of single wings in container experiments. Data are shown as box plots with means (diamond), medians (horizontal bar), quartiles (hinges) and whiskers extending to the most extreme data point no further than 1.5 times the interquartile range away from the box. The notches extend to ±1.58 interquartile range divided by $\sqrt{n}$, where n is the number of data points. Outliers are plotted as open circles. (C) Relationship between body mass m and area of single wings. Lines are linear regression fits (A_0=am+b; females: a=0.2 mm² mg^{-1}, b=6.1 mm², R^2=0.48; males: a=0.3 mm² mg^{-1}, b=5.1 mm², R^2 = 0.63). (D) Mortality of flies used for analysis (N=20 females, N=35 males) in container experiments (means±range). (E) Wing area and (F) mortality of flies in free-flight experiments (N=8 females, N=9 males).

Physiological and chronological age

For age-related phenomena, the physiological age can be more relevant than the chronological age (Burkhard et al., 2002; Hayes et al., 1998). We thus used physiological age in this study and estimated its value in degree days (Kelvin days, K days) above a threshold temperature of 11°C (Skovgård and Nachman, 2004). Temperature was continuously scored and eventually averaged for each 12 h light or dark period. Missing values were interpolated. Fly hatching was monitored twice a day. Physiological and chronological age are linearly correlated with a Pearson's correlation coefficient of >0.99. Mean linear regression slope between chronological and physiological age was 15±3 K and varied between ∼10 K and 18 K (container experiments). The slope in the free-flight experiment was ∼13 K. For correlations between physiological and chronological age, see Supplementary Materials and Methods 1. The theoretical maximum precision in physiological age estimation was 6.75 K days and mean ambient temperature for all measurements was ∼24.5°C.

Container experiment setup

The experimental setup consisted of nine cylindrical plastic containers that were mounted in 3×3 holes of an acrylic glass rack. All containers except for the water supply were surrounded by a printed random dot visual environment and equipped with an electret microphone at the bottom (Fig. 1C). Other containers served as the water supply, reference for sound recording (empty container) and fly reservoir to replace flies that died in one of the six experimental containers. All containers were closed with foam stoppers. The rack was illuminated from above by two fluorescent lamps (16 W, colour temperature 3400 K) on a 12 h:12 h day:night cycle (07:00–19:00 h). Measured illuminance inside the containers varied between 380 and 840 lx. We monitored ambient temperature (mean 24.7±2.8°C) and relative humidity (mean 38±6%) every 5 min with a data logger (BL-30, Trotec GmbH, Heinsberg, Germany).

To monitor the animals' flight activity inside the containers, we recorded the flight sound from seven microphones on the rack using a multi-channel audio interface (Tascam US-16x08, TEAC Europe GmbH, Wiesbaden-Erbenheim, Germany). Sound was sampled at 44.1 kHz, bandpass filtered, and subsequently down-sampled to 8.0 kHz (MediaHuman audio converter; see Supplementary Materials and Methods 2 and 3 for further details). We determined flight activity from the difference between the audio signal inside containers with flies and the sound reference container without flies using custom-written Python script. The software filtered (6th order Butterworth bandpass, 100 Hz to 1000 Hz) the signals, converted them to absolute values (rectification), and subsequently smoothed them with a 0.01 s boxcar averaging filter. Flight was counted when the flight signal amplitude was at least twice the sound amplitude of the control container. Processing of data (∼1.3 terabytes, TB) was performed on a node of the Skylake partition of Irene supercomputer (48 CPU cores, 180 GB RAM; TGCC at Bruyères-le-Châtel, France). Six audio tracks were simultaneously processed and total processing time was approximately 3 h. To exclude short locomotor hops, we only considered flights with a minimum duration of 0.03 s, i.e. ∼5 wingbeats at ∼170 Hz flapping frequency. To link the audio signal to flight activity, we conducted control experiments using high-speed video and sound recording. These controls showed that, on

average, a flight sound (flight bout) was due to flight of one out of the four flies inside each container (see Supplementary Materials and Methods 3 for further details). Normalised flight activity for a group of four flies, $\hat{t}_{\text{flight}}$, during a recorded time span Δt_{rec} was calculated from the ratio between flight Δt_{flight} and recording time Δt_{rec}. This measure is expressed by the following equation:

$$\hat{t}_{\text{flight}} = \frac{\Delta t_{\text{flight}}}{\Delta t_{\text{rec}}}. \quad (1)$$

For estimation of flight activity, Δt_{rec} was ∼12 h and for circadian rhythm analyses it was ∼15 min. We interpolated flight activity data that were missed during wing area measurements, noisy audio signalling or other technical problems.

One of our initial ideas was the reconstruction of wing beat frequency from the sound recordings during flight. However, simultaneous high-speed video analysis on wing motion and sound recording revealed that the major frequency component obtained from fast Fourier analysis did not reliably map wing flapping motion. Possible explanations include sound interference between the two beating wings, sound being reflected within the container and Doppler effects. We thus excluded the frequency analysis from this study.

Free-flight experiment setup

To score the relationship between wing damage and locomotor capacity, flies were kept and tested in the mesh flight cage under similar environmental conditions to those used for the container experiments. Mean illuminance inside the cage was ∼350 lx at the bottom and 42,000 lx at the top, mean ambient temperature was 24.1±0.8°C, and relative humidity was 41±7%. Each time we removed the flies from the cage in order to take photographs of the wings, we tested their ability to support their body weight in free flight over a flight distance of 26 cm by releasing them in the middle of the cage. Weight-supporting active flight was considered when the altitude of the landing site was equal to or above the altitude of the start post.

Estimations of wing area and damage

In both experimental approaches, we estimated wing wear on average 3 times a week (Monday, Wednesday, Friday) throughout the animals' lifetime. The animals were removed from their housing, cold-anaesthetised at ∼4°C and placed under a stereomicroscope that was equipped with a camera (Canon EOS 750D, Canon, Tokyo, Japan). We traced the wing planforms using Fiji (Schindelin et al., 2012) and stored them as binary wing images (wing mask). For estimation of total area and alignment during post-processing, we manually marked three positions for reference in all left and right wings on the photos (P_1–P_3, red area in Fig. 1B) and used them to align the wing masks using custom-written scripts in R and Python. Wing root and alula could not be reliably traced. Therefore, we only traced the area distal to the line between P_2 and P_3 (white area in Fig. 1B; see Supplementary Materials and Methods 4 for further details). For estimations of the 2nd moment of wing area, we added an averaged sex-specific area to represent the wing proximal to the line between P2 and P3 (excluding the alula), and used mean root positions and longitudinal axes determined from the intact wings in all cases, i.e. in both intact and damaged wings (see Supplementary Materials and Methods 5 for further details). Wing damage is the relative wing area of a single wing $\hat{A}$ expressed by:

$$\hat{A} = \frac{A}{A_0}, \quad (2)$$

where A is the sum of area-covering image pixels and A_0 is the initial wing area at the beginning of the experiment (traced area only, white in Fig. 1B). As left and right wings mostly have different damage and thus area, we used a modified version of Ellington's (1984) theoretical derivative for 2nd moment of total wing area for a single wing (see Supplementary Materials and Methods 6 for further details):

$$A_2 = \int_{r=0}^{R} c(r) r^2 \mathrm{d}r, \quad (3)$$

where R is the wing length, r is the position along the axis from wing root to wing tip and $c(r)$ is the wing chord at position r. Total area of both wings (S) and body mass-specific 2nd moment of area of both wings (S_2^*) are derived as the sum of both wings. Total normalised wing area ($\hat{S}$) is the sum of left and right wing area divided by the sum of both initial areas. The relative right-minus-left difference of total wing area is:

$$\Delta\hat{S} = \frac{\hat{A}_{\text{right}} - \hat{A}_{\text{left}}}{\hat{A}_{\text{right}} + \hat{A}_{\text{left}}} \quad (4)$$

and the difference of the 2nd moment of area is:

$$\Delta S_2^* = \frac{A_{2,\text{right}} - A_{2,\text{left}}}{A_{2,\text{right}} + A_{2,\text{left}}}. \quad (5)$$

Both parameters are normalised by the sum of both wings and can be used as a measure for damage asymmetry. A similar description of asymmetry has previously been used (Johnson and Cartar, 2014).

Progression of wing damage

Previous studies suggested that wing area loss exponentially increases (Higginson and Gilbert, 2004) or asymptotically saturates (Mountcastle and Combes, 2014) with increasing lifetime of an insect. Our wing area data suggest a combination of both exponential relationships that is best described by a four-parameter logistic function:

$$\hat{A}(t) = \frac{\hat{A}_{\text{f}} - \hat{A}_0}{1 + e^{k(t_{\text{tp}} - t)}} + \hat{A}_0, \quad (6)$$

where $\hat{A}_0 = 1$ is the normalised initial area, $\hat{A}_{\text{f}}$ is the final normalised wing area at the animal's death, t_{tp} is the x-coordinate of the inflexion point of the logistic function at 50% of the final area loss $\hat{A} = \frac{1}{2}(\hat{A}_0 + \hat{A}_{\text{f}})$, t is time and k is the logistic growth rate, defined as:

$$k = 4\frac{\mathrm{d}\hat{A}/\mathrm{d}t(t_{\text{p}})}{\hat{A}_{\text{f}} - \hat{A}_0}. \quad (7)$$

For time t in Eqns 4 and 5, we either inserted physiological age or cumulative activity. Cumulative activity was calculated from flight activity bouts in each fly group, divided by the number of individuals in the container. This procedure was developed according to control experiments (see Supplementary Materials and Methods 7). We fitted the model parameters using Gauss–Newton or Levenberg–Marquardt algorithms depending on which worked best. We defined the beginning of wing area loss (t_{f}; Fig. 1D) as the value of the logistic function at which wing area falls below 0.85 initial wing area. This threshold was derived according to maximum measurement noise in all flies and was ±∼15% of initial wing area.

Statistics

General concept

Our statistical analyses cover approaches on two topics of this study. The first topic was the relationship between wing area loss, physiological age and flight activity (container experiments) and the

Journal of Experimental Biology (2022) 225, jeb242872. doi:10.1242/jeb.242872

second topic was the relationship between wing area loss and flight capacity (free-flight experiments). The statistics on the first topic consist of three steps: (i) a pre-test procedure using Pearson correlation, (ii) a principal component analysis (PCA) with Kolmogorov–Smirnov test, and (iii) a comparison of model parameter variability to assess the significance of physiological age and flight activity on wing area. The statistics on the second topic encompassed PCA only.

Correlation of a combined predictor

To pre-evaluate any relationship between wing area loss and the two predictors (physiological age and cumulative flight activity), we tested whether t_f values at $0.85\hat{A}_0$ derived from the logistic fits are clustered compared with a reference distribution. A clustered value would suggest that wing area loss starts at a specific combination of age and activity during the animals' lifetime. A limitation of this approach is that it excludes all wings for which we could not conduct a logistic fit, for example all wings with less than 15% area loss (see above). Area loss of less than 15% prevented fitting a curve in ∼80% female and ∼35% male wings. For analysis, we reduced the two dimensions age and activity to one dimension using PCA. The magnitude of the first principal component (PC1) for all area measurements in all flies was used as a reference. As the units of the two predictors are different (age, K days; activity, h), age and activity were z-transformed by subtracting means and normalising to standard deviation before PCA. The reference distribution takes into account the various lifespans because the number of age and activity data points decreases with increasing age and activity in the tested flies (Fig. 2D,F). In other words: it considers the changes in local density of PC1-values due to the decreasing number of flies alive with increasing time. To directly compare reference values along PC1 with t_f values from the logistic fits, we z-transformed t_f values for age and activity using the means and standard deviations of the reference dataset, copied the PC1 eigenvector of the reference PCA into the t_f coordinate system instead of performing a new PCA, and estimated PC1 t_f values along the eigenvector. To test for statistical differences between the reference and t_f distributions along PC1, we used a Kolmogorov–Smirnov test with Bonferroni correction for multiple testing.

Comparison of model parameters between dimensions

PCA cannot provide evidence for the strength of each predictor for wing damage. We approached this problem by comparing the variance of the beginning of wing damage (t_f) between both predictors. The t_f values were derived from the logistic wing models fitted according to age and activity, respectively. If the models are more uniform along one dimension, this dimension would appear to be a better predictor of wing damage. As the two predictors possess different scales, we transformed the two sets of t_f values using their medians for centring them on zero and normalising their scale. After transformation, data variability was relative to the original scale and the variance of both datasets was compared by the Fligner–Killeen test on homogeneity of variances. The above approach is limited to those wings for which a logistic curve could be fitted successfully (∼15% for activity as a predictor and 20% for age as a predictor for female wing models, ∼50% for male models in both cases). This excludes wings with less than 15% wing area loss (which is the case for 80% of female wings and 35% of male wings) and wings where the fitting process was unsuccessful for other reasons. An alternative approach that allowed us to include all measured data such as multiple linear model regression analysis was not suitable because of the logistic development in wing area loss.

RESULTS

Life expectancy

In the container experiment, females reached physiological (chronological) ages of between 310 and 880 K days (17.5 and 59.5 days); mean age was 480±140 K days (32.0±11.5 days; Fig. 2D). Females lived ∼1.5 times longer than males (two sample t-test; physiological age, $P<0.001$; chronological age, $P<0.01$), which reached maximum ages of between 30 and 660 K days (2.0 and 49.5 days); mean age of these flies was 320±170 K days (22±12 days; Fig. 2D). In the free-flight experiments, female flies lived 400–1210 K days (31 to 92.5 days) with a mean of 860 ±270 K days (65.5±20.5 days; Fig. 2F). In contrast to the container experiment, the life expectancy of males in the free-flight cage was relatively shorter but not significantly different from that of females (two-sample t-test, $P>0.09$ for both ages) and ranged from 400 to 930 K days, with a mean age of 650±180 K days (31 to 70.5 days; 50.0±13.5 days). In sum, flies in the free-flight experiment tended to live twice as long as those in the container experiment.

Fly activity in containers

In total, we recorded 7,776,670 flights of which ∼30% were measured in containers with females and ∼70% with males (Fig. 3). Fig. 3A shows frequency and length of flight bouts and how they were distributed over one day. Mean duration of flight bouts in females was 0.20±0.23 s, significantly longer than that in males (0.17±0.17 s; Wilcoxon rank sum test with continuity correction, $P<0.001$). Fig. 3B highlights that ∼75% of all flight sequences were equal to or shorter

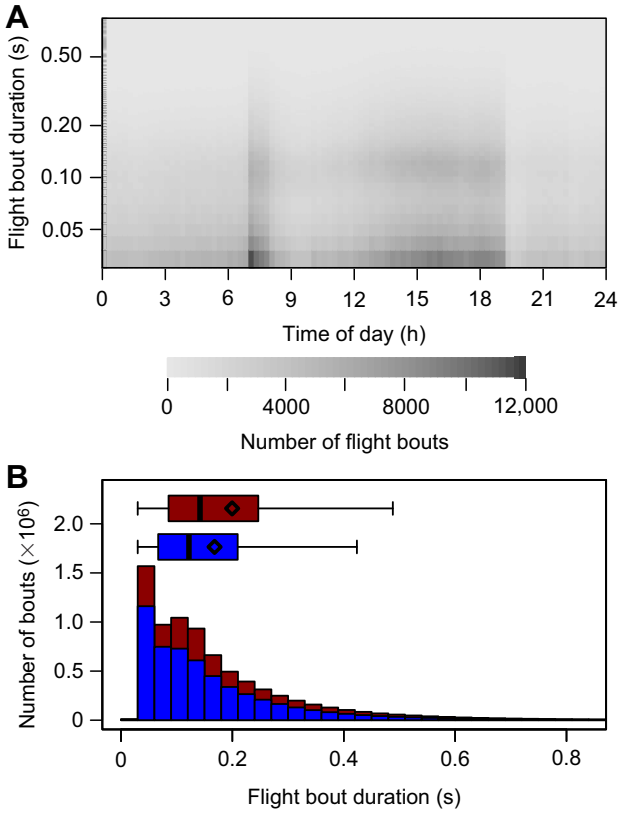

Fig. 3. Duration of flight sequences inside the flight containers. (A) Number and length of single flights over the course of the day. Numbers are plotted as greyscale. (B) Histogram of flights according to the duration of flight bouts and sex (red, female; blue, male). Data cover ∼99% of all recorded activity bouts and box plots show medians (solid lines) and means (diamonds). See also legend to Fig. 2 for box plot explanation (outliers not shown).

Journal of Experimental Biology (2022) 225, jeb242872. doi:10.1242/jeb.242872

than ~200 ms (females, ~74.8%; males, ~74.6%). The 99% quantiles in flight activity bout durations thus yield 0.92 s in females and 0.79 s in males. The ethogram in Fig. 4 shows that activity bouts were not equally spaced in time, owing to the animals' circadian rhythm (Fig. 4A). Flight activity during the light period was significantly higher than activity during the dark period (paired *t*-test, $P<0.001$; Fig. 4B). The data also show that males were significantly more active than females during both the light (females, $\hat{t}_{\text{flight}} = 0.054 \pm 0.019$; males, $\hat{t}_{\text{flight}} = 0.093 \pm 0.037$) and dark period (females $\hat{t}_{\text{flight}} = 0.007 \pm 0.005$; males, $\hat{t}_{\text{flight}} = 0.034 \pm 0.010$; Welch two-sample *t*-test, $P<0.05$; Fig. 4C).

Pattern and progression of wing damage

Although the two experimental approaches (container, free flight) provided separate datasets for wing damage, we summarise these findings in this section. Fig. 5 shows two examples of wing damage for six observations of two different flies for container (male; Fig. 5B) and free-flight experiments (female; Fig. 5A). In total, we were able to score wing damage in 534 and 656 photos in container experiments and 190 and 157 photos in free-flight experiments of females and males, respectively. Wing wear typically started in both sexes by a loss of wing area at the wing tip or the distal parts of membrane area at the trailing wing edge. At this initial state, we did not observe any area loss at the leading edge in either sex. With increasing age, the wings also broke at the stiff leading edge and typically lost all distal areas. Thus, wing length decreased with increasing age and flight activity.

As mentioned in Materials and Methods, we used a logistic fit function to describe wing area loss in a subset of all data. The examples of this analysis show fast (Fig. 6A–C) and slow (Fig. 6D,E) damage progress. In general, the results of the logistic fit suggest that wing area loss occurs suddenly and quickly progresses with age and activity (Table 1). As already mentioned, the analysis condition excluded single wings (container experiment) and sets of wings of individual animals (free-flight experiment) that experienced less than 15% wing area loss, i.e. 33 female and 24 male wings in container experiments and 2 females and 1 male in free-flight experiments. These values correspond to ~83% and ~34% of the tested female and male wings in container experiments and ~25% of females and ~11% of males in free-flight experiments, respectively. For the predictors physiological age and cumulative activity, we eventually derived data from 7 and 6 female wings, and 37 and 37 male wings, respectively, which is 40% of all tested wings in container experiments. For the 6 females and 8 males available for fitting a curve in the free-flight experiment, one model per fly could be fitted successfully (~82% of all flies).

We used these models as the basis for further analysis. In the container experiment, we found that wings lost on average 69% of their initial area within the flies' lifetime ($\hat{A}_t$=0.31±0.23 initial area). Area loss in single animals was widely scattered, ranging from ~100% (complete area loss) to a minimum of ~15% loss of initial area (container experiments) at death. We obtained similar data for

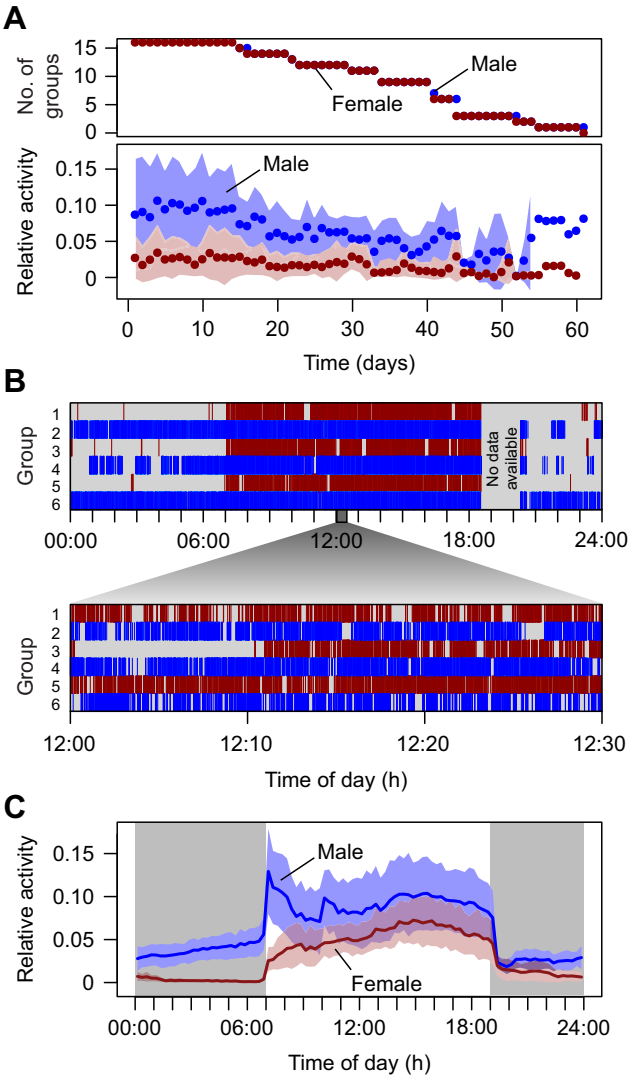

Fig. 4. Ethogram of flight activity in containers. (A) Bottom: mean relative activity (ratio of activity to total time) after interpolation of all tested fly groups plotted against time (shaded areas are standard deviation). Top: number of fly groups (N=7 containers with females, N=9 containers with males). (B) Flight activity (vertical lines) of 6 groups of approximately 8 day old flies scored over 24 h (top), with a close up at one 30 min interval (bottom). (C) Means±s.d. of circadian activity. Flight activity (N=5760 data for each sex) was estimated in 15 min time segments (no interpolated data). Grey area is night-time without illumination. Female groups are plotted in red and male groups in blue.

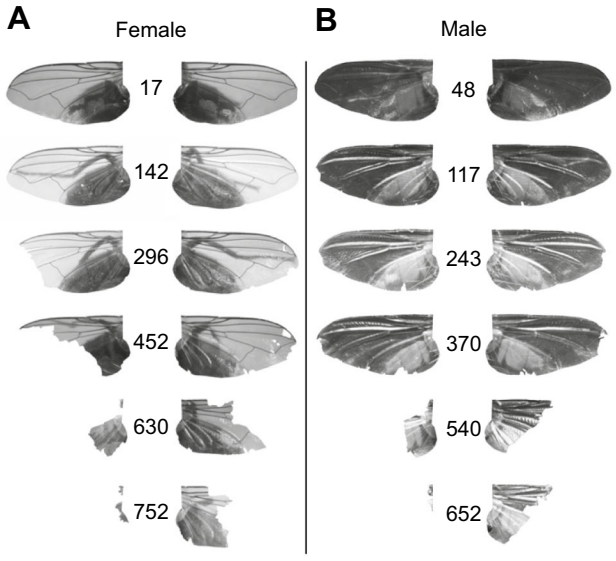

Fig. 5. Loss of wing area in the two experimental approaches for a single fly each at different physiological ages. Loss of wing area scored as a function of age (K days) in (A) free flight (female) and (B) container experiments (male). In total, throughout the animals' lifetime, we determined wing area for 594 left and 596 right wing photos in container experiments and 350 left and 348 right wing photos in free-flight experiments.

Journal of Experimental Biology (2022) 225, jeb242872. doi:10.1242/jeb.242872

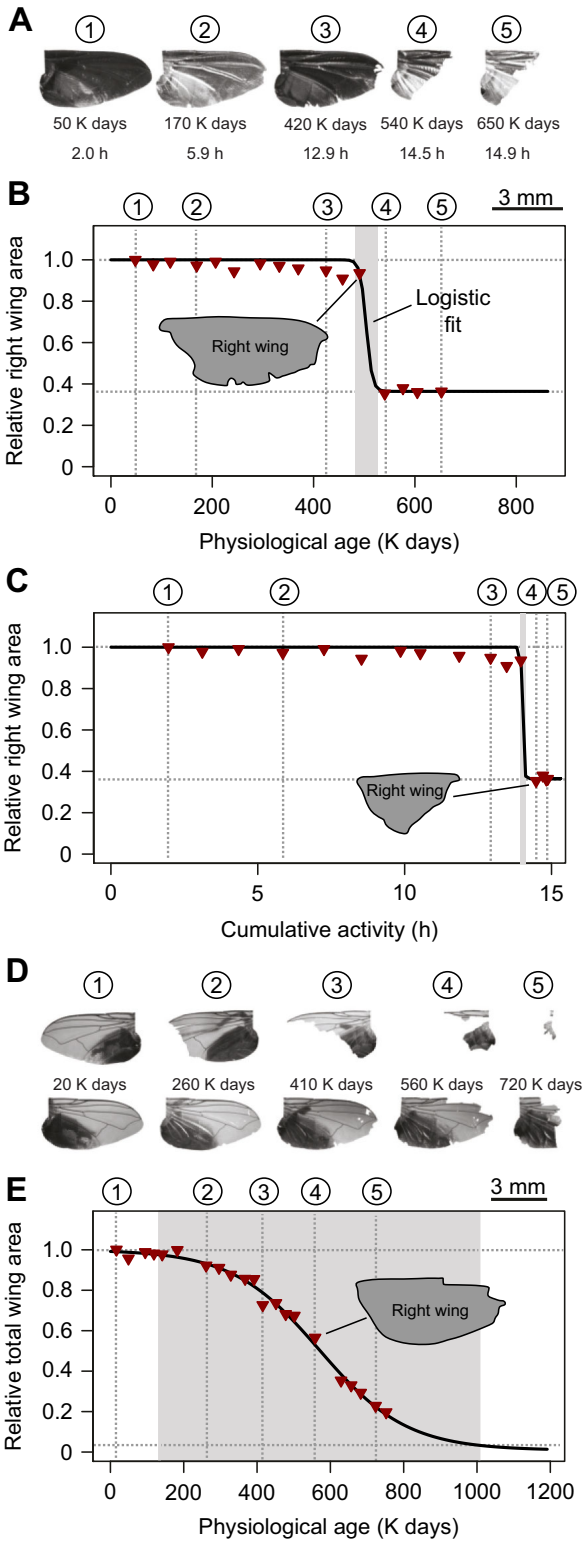

Fig. 6. Development of wing area loss in single house flies. Wing area was normalised to initial wing area after hatching. (A) Progress in area degradation in the right wing of a male in the container experiment. Values are physiological age (top) and flight activity (bottom). (B,C) Relative wing area (red) of the animal in A plotted against the two predictors (B, physiological age; C, flight activity) and logistic fit to the data (black). (D,E) Loss of wing area in both wings of a female tested in free-flight experiments (D), and relative wing area plotted against physiological age (E). Grey shaded areas and dashed horizontal lines indicate the progress of wing damage.

flies in the flight cage (free-flight experiments) in which the mean sum of left and right wing area at death (Eqn 4) was ∼27% of the initial area ($\hat{S}_f = 0.27 \pm 0.35$) and ranged from ∼100% to ∼16% loss of initial area. The time at which the flies lost 50% of their wing area loss, i.e. the inflexion point of the logistic fit function, was ∼258±165 K days for physiological age and ∼6.72±5.13 h for flight activity (container experiments), compared with ∼614±266 K days in free-flight experiments (Table 1). The data in Table 1 also highlight that flies in small containers lost wing area ∼20 times more rapidly compared with their relatives in the larger flight cage. We found that the rate of wing area loss at the inflexion point was $\sim -31.4(\pm 36.8)\times 10^{-3}$ K^{-1} day^{-1} for physiological age and $\sim -2.68\pm 4.46$ h^{-1} for accumulative flight activity, compared with $\sim -1.59(\pm 1.05)\times 10^{-3}$ K^{-1} day^{-1} in free-flight experiments. Logistic growth rates were broadly independent of the onset of wing damage (Fig. 1D) in both container (linear regression, flight activity versus k; $R^2<0.16$) and free-flight experiments [flight activity versus k, $R^2<0.01$; where k is the logistic growth rate (see Eqns 6,7)].).

Flight activity and wing damage

Wing damage may depend on age or activity, a combination of the two, or neither. We approached this question by scoring the variance of the relationship between age and activity in each animal. Without variance, age and activity would be indistinguishable. This was checked using a linear interaction model with activity as outcome variable, age as covariate and individual fly identity as explanatory factor (Fig. 7A). We estimated regression slopes and intercepts of 53 animals and found a mean slope of ∼0.020±0.009 h K^{-1} day^{-1} for all flies. The slope varied between ∼0.005 h K^{-1} day^{-1} (Fig. 7A, yellow) and 0.042 h K^{-1} day^{-1} in single animals (Fig. 7A, cyan). The mean regression intercept was ∼0.21±0.71 h and close to zero, with a variability ranging from −1.36 to 2.07 h. Age, individual fly identity and their interaction were significant model terms, suggesting that both slopes and intercepts were generally different among flies ($P<0.001$). Pearson's correlation coefficient on pooled flies was ∼0.71 (625 data points, $N=20$ females, $N=35$ males) and smaller than the coefficients for single animals, which ranged from ∼0.97 to ∼1.0.

Firstly, we combined the two predictors and analysed to what degree this one-dimensional combination is correlated with wing damage. Because of the elevated degree of collinearity between the two predictors, this approach allowed us to analyse dependencies regardless of whether the two predictors could be disentangled. PCA on the combined predictors was done on 1250 data points of which 558 were recorded in females and 692 in males. The lower and upper quartiles of physiological age range from 120 to 370 K days in females and from 80 to 290 K days in males, and flight activity from 0.92 to 3.99 h and from 1.96 to 8.53 h, respectively. The first principal component (PC1) explained ∼86% of the data variance. Fig. 7B shows that after z-transformation, approximately 50% of PC1 values were distributed between −1.13 and 0.57 in females and between −1.08 and 1.09 in males. Calculations further yielded t_f=450±60 K days and 4.68±1.13 h in females, and 210±130 K days and 6.32±3.88 h in males, respectively. After projecting these values into PCA space, ∼50% of PC1 varied between 0.69 and 1.50, and −0.82 and 1.07 in females and males, respectively. We found no significant difference between the reference distribution and the distribution of t_f in pooled flies ($P=0.172$). This result, however, was sex specific because in females the difference was significant ($P<0.05$) while in males it was not ($P=1.00$). We also found that females and males differed in the reference distribution ($P<0.05$) but not in the distribution of t_f ($P=0.2$, Bonferroni correction, $N=5$ tests).

Journal of Experimental Biology (2022) 225, jeb242872. doi:10.1242/jeb.242872

Table 1. Statistics of logistic fits to wing damage data

Experiment	Time	Sex	$\hat{A}_f$	t_{tp}	t_f	Slope at t_{tp}	N	N_{data}	P_{succ}
Container	Age	f, m	0.31±0.23	258±165 K days	230±180 K days	−31.4±36.8 10^{-3} K^{-1} day^{-1}	43	521	40%
Container	Activity	f, m	0.31±0.23	6.72±5.13 h	5.99±4.18 h	−2.68±4.46 h^{-1}	43	515	39%
Free flight	Age	f, m	0.27±0.35	614±266 K days	486±214 K days	−1.59±1.05 10^{-3} K^{-1} day^{-1}	14	263	82%
Container	Age	f	0.27±0.32	405±208 K days	333±348 K days	−33.2±39.2 10^{-3} K^{-1} day^{-1}	7	109	18%
Container	Activity	f	0.31±0.33	3.95±2.34 h	3.22±3.69 h	−4.31±7.97 h^{-1}	6	89	15%
Free flight	Age	f	0.14±0.34	723±302 K days	538±264 K days	−1.55±0.97 10^{-3} K^{-1} day^{-1}	6	122	75%
Container	Age	m	0.31±0.22	230±142 K days	210±126 K days	−31.1±36.9 10^{-3} K^{-1} day^{-1}	36	412	53%
Container	Activity	m	0.31±0.21	7.18±5.34 h	6.44±4.13 K days	−2.42±3.72 h^{-1}	37	426	53%
Free flight	Age	m	0.37±0.33	532±220 K days	447±176 K days	−1.61±1.18 10^{-3} K^{-1} day^{-1}	8	141	89%

Initial wing area A_0 was always set to 1.0. $\hat{A}_f$, wing area at death normalised to A_0; t_{tp}, physiological age or cumulative activity at inflexion point; t_f, age or activity at $0.85A_0$; N, number of tested models; N_{data}, total number of data points used in statistics; P_{succ}, percentage of successful logistic fits to the tested models.

Secondly, we tested the two predictors as separate variables by comparing the relative variability of t_f for age and activity (see Materials and Methods). We found that the median of model deviance divided by degrees of freedom was 1.15×10^{-3} for physiological age (N=44 wings) and 1.14×10^{-3} for cumulative activity (N=43 wings). These values were not significantly different (two-sided two-sample Kolmogorov–Smirnov test, $P\approx0.89$). This result suggests that wing damage might depend more on age than activity or vice versa if variability of model parameters is different for the two predictors, because the modelling did not obviously work better along one dimension than the other. We thus compared the relative variability of t_f between predictors and found no significant difference between the two values (P=0.807, Fligner–Killeen test). This means that wing damage in the subset of successfully modelled wings cannot be attributed to a single predictor.

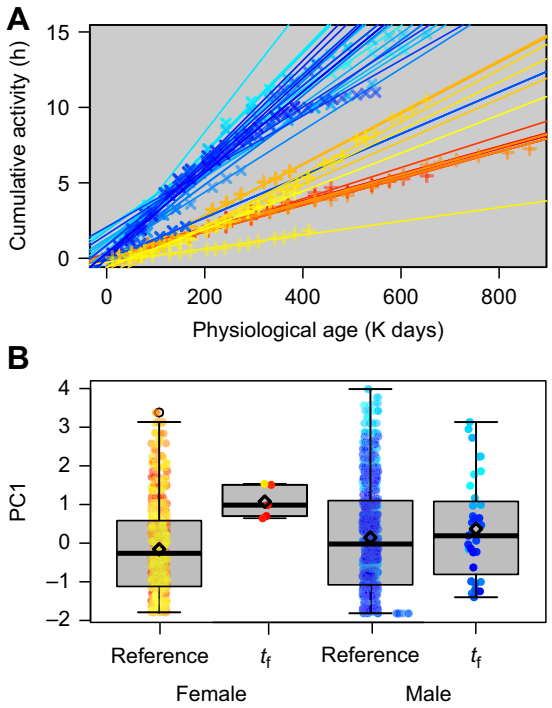

Fig. 7. Flight activity and age in females and males. (A) Relationship between accumulated flight activity and physiological age in container experiments. Individual flies are plotted in colour, with females plotted by yellow–red upright crosses and males by cyan–blue tilted/inclined crosses. Lines are linear regression fits to the data. (B) Principal component analysis (PCA). Data show box plots with superimposed first principal component (PC1) data of reference (left side) and t_f (right side) for females and males, respectively. Flies are colour coded as shown in A. See Materials and Methods for more detailed explanations.

Flight ability and wing damage

Fig. 8 shows how wing area loss developed in house flies that lived in the large flight cage (free-flight experiment; analysis for this experiment was done at the animal level). These data potentially link wing damage to the animals' free-flight capacity. According to quasi-steady aerodynamic theory (see Discussion), lift production depends on wing area and increases with the wings' 2nd moment of area (Weis-Fogh, 1973). In general, our data show that normalised wing area [linear regression, $\hat{S}(\theta) = a\theta + b$; $a = -1.22\times10^{-4}$ $K^{-1}day^{-1}$, $b = 0.96$, R^2=0.05, P_{slope}<0.01, N=347; Fig. 8A] and mass-specific 2nd moment of area [linear regression, $S_2^*(\theta) = -5.0\times10^{-3}K^{-1}day^{-1}\,\theta + 33.4\,mm^4\,mg^{-1}$, R^2=0.03, P_{slope}<0.01; Fig. 8B] decrease with increasing age (θ). In most flies, the same also held for normalised right minus left differences of these measures (Fig. 8C,E). Fig. 8D highlights the linear relationship [linear regression, $S_2^*(\hat{S}) = a\hat{S} + b$; $a = 48.39\ mm^4\ mg^{-1}$, $b = -12.51\ mm^4\ mg^{-1}$, R^2=0.85, P_{slope}<0.001] between wing area and mass-specific 2nd moment of area – flies with wing damage thus suffer from simultaneous changes in lifting-surface and wing aspect ratio with increasing age. The relative right minus left difference in wing area is largely independent of total normalised wing area until area drops below a threshold of ∼0.8 area (Fig. 8F).

Free-flight performance was sorted into only two categories ('flight', 'non-flight'). We scored wing area for 347 out of 351 flight trials (192 trials, N=8 females; 159 trials, N=9 males) that split into 308 'flight' and 43 'non-flight' scores (Fig. 9). Fig. 9A shows that the age distribution of flying flies (median: ∼370 K days) is significantly different from the age distribution (median: ∼560 K days) of non-flying flies (two-sided two-sample Kolmogorov–Smirnov test, P<0.001, Bonferroni-corrected for 6 tests, N=351). The same holds for normalised wing area and mass-specific 2nd moment of area in both categories (medians: ∼0.97 versus ∼0.63, Fig. 9C; 33.1 versus 19.9 $mm^4\ mg^{-1}$, Fig. 9D; one-sided two-sample Kolmogorov–Smirnov test, P<0.001, Bonferroni-corrected for 6 tests, N=347). The reverse applies to absolute normalised differences of both parameters (medians: ∼0.01 versus ∼0.41, Fig. 9E; 0.02 versus 0.64, Fig. 9F, P<0.001). Similar to the analysis of the container experiment, we calculated the PC1 as a predictor for wing area loss using PCA on z-transformed normalised wing area, body mass-specific 2nd moment of area and absolute relative differences. PC1 accounted for 88% of the variance and medians were −0.78 (flight) and 3.43 (non-flight; Fig. 9B). We found that flight and non-flight distributions of PC1 were significantly different (two-sided Kolmogorov–Smirnov test with Bonferroni correction, P<0.001, N=347).

Journal of Experimental Biology (2022) 225, jeb242872. doi:10.1242/jeb.242872

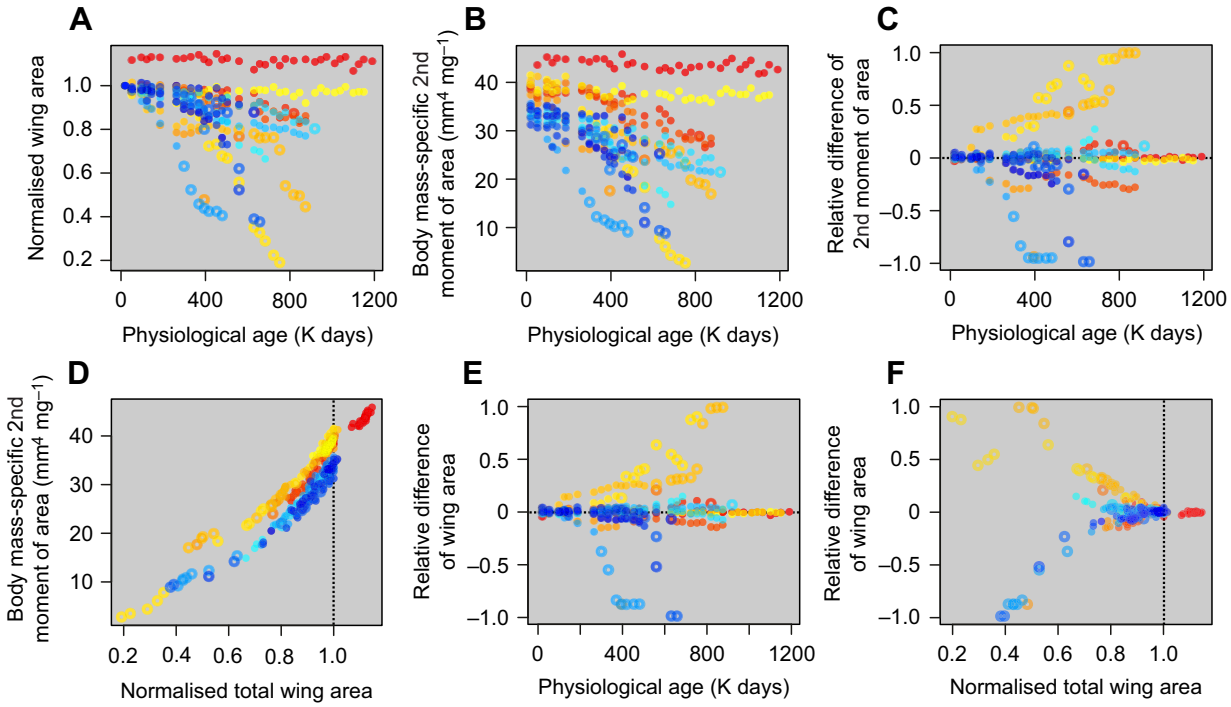

Fig. 8. Relationships between wing area, 2nd moment of wing area and age in free-flight experiments for 'flight' (solid circle) and 'non-flight' (open circle) trials. Individual flies are colour coded as in Fig. 7. Data are plotted as follows: (A) normalised area of both wings ($\hat{S}$), (B) body mass-specific 2nd moment of wing area (S_2^*) and (C) right minus left wing difference in S_2^* normalised to the sum (ΔS_2^*), all plotted against physiological age. (D) The 2nd moment of wing area (S_2^*) linearly increases with increasing normalised total wing area. (E) Relative right minus left difference in wing area increases with age. (F) Right minus left area asymmetry normalised to the sum increases with decreasing wing area.

DISCUSSION

General aspects

Flight by active wing flapping is one of the most costly forms of locomotion (Casey and Ellington, 1989). Consequently, any change in the flight apparatus such as wing area and shape may compromise flight ability and efficiency and thus have serious consequences for the animal's fitness. To highlight the significance of wing area loss, we here investigated the factors that determine wing damage in house flies and scored the ability of these flies to fly with damaged wings. In contrast to previously published experiments in which wings of flies were artificially cut (e.g. Higginson et al., 2011; Mountcastle et al., 2016; Muijres et al., 2017; Roberts and Cartar, 2015), we investigated natural progression of wing damage under two housing conditions. One focus of the study was to map the progression of damage and to describe wing area loss throughout the animal's entire lifetime as a function of age and flight activity. We found that (i) wing damage typically starts to occur at the wing tip and progresses in a characteristic pattern (Figs 5 and 6), (ii) the rate of wing damage is independent of both age and activity at the initial area change, (iii) physiological age and flight activity are both predictors for wing damage, (iv) flight activity patterns are different between females and males (Figs 2–4), and (iv) the flies' ability to produce forces for body mass support decreases with increasing age and decreasing wing area, shape and asymmetry between the two wings (Figs 8 and 9). Noteworthy, as age, flight activity and wing damage simultaneously change, the loss of flight ability probably results from various factors of which we only scored a small number.

Impact of housing conditions

Investigations on flies kept in cages previously showed that behaviour and life history change depending on housing conditions. The life expectancy of house flies depends strongly on activity, which is shaped by temperature, population density and sex ratio (Ragland and Sohal, 1973, 1975; Sohal and Buchan, 1981). To account for these factors, we monitored temperature throughout the measurements and used physiological age which considers temperature rather than the chronological age as a descriptor. Sex ratio was considered by keeping females and males in separate containers. It is obvious that higher population density increases the likelihood of wing collisions in flying animals. For this reason, we selected two housing conditions with vastly different population densities. Fig. 2 shows that house flies kept in the larger cage lived considerably longer and tended to have larger wing areas. The latter result might be due to the variance in rearing conditions because all tested flies stem from the same population. The longer lifespan of flies in the free-flight experiment is consistent with the idea that crowded housing conditions, elevated levels of activity and an elevated number of males in a group result in earlier senescence. Ragland and Sohal (1973), for example, showed that under certain conditions, male house flies without wings perish earlier than intact animals. The authors contributed this finding to leg muscle failure because of extended mating behaviour (see Introduction). This is also consistent with elevated longevity in less-active flies (Sohal and Buchan, 1981). Even if flies live longer, older flies do not necessarily retain their flight ability for longer. Lane et al. (2014) showed that flies with forced activity stopped flying earlier in their life than flies that were voluntarily active. Our data on flight activity might be shaped by these findings because the flies inside the container and the cage were continuously stimulated by flying conspecifics. This might explain the earlier onset of wing damage in the container compared with the free-flight experiment. Altogether, males are more likely to experience wing damage

Journal of Experimental Biology (2022) 225, jeb242872. doi:10.1242/jeb.242872

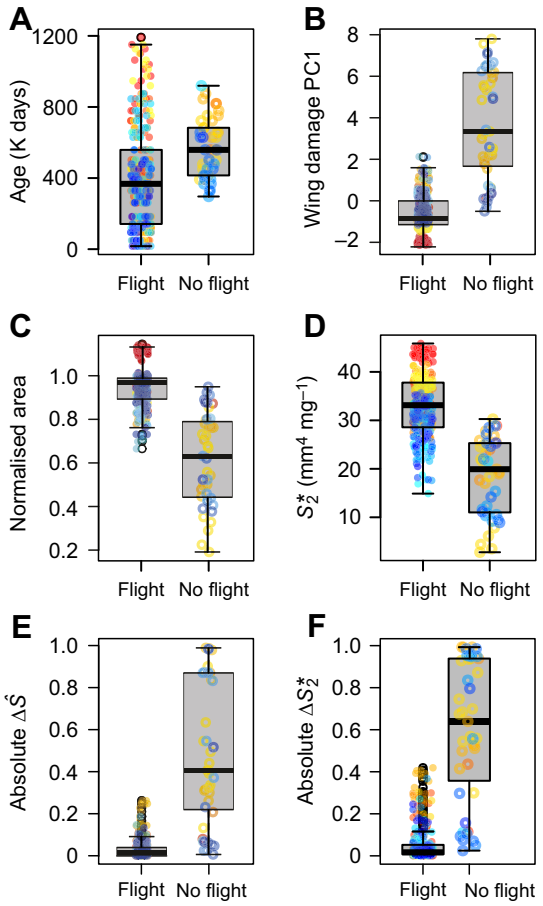

Fig. 9. Comparison of wing area measures in flying (solid circle) and non-flying (open circle) house flies. Data are shown as box plots and data for individual flies are plotted in colour. (A) Physiological age in both groups. (B) First principal component of wing measures. (C–F) Data for total wing area (C) and 2nd moment of area including their relative right minus left differences (S_2^*, D; $\Delta\hat{S}$, E; and ΔS_2^*, F). See legend to Fig. 2 for explanation of box plots.

than females, especially when males are kept in groups (Sohal and Buchan, 1981).

Pattern and development of wing area loss

In nature, many insect wings are damaged, but in only a few cases is the damage severe (Anderson and Keyel, 2006; Rajabi et al., 2017; Rehan and Richards, 2010). To compare the damage pattern in our house flies with that of animals living in nature, we collected flies from the field between July and September 2018 using nets and traps at different horse stables around the University of Rostock, in Rostock Zoo, and around a house in Güstrow, Germany. Wing damage in these flies showed similar patterns to those in our experiments but damage was typically less pronounced. Typical patterns showed a loss of wing area at the wing tip and the membranous wing's trailing edge, similar to the wings shown in Figs 5 and 6. In total, 65% (161) of the trapped animals had intact wings, 24% (60) had only small damage and only 4% (10) of animals showed elevated wing damage. The finding that wing wear starts at the wing tip and trailing edge is also consistent with previous findings on bumblebees (Cartar, 1992). Moreover, Rajabi et al. (2017) reported wild dragonflies with both small (∼10% area loss) and severe damage in single wings with a loss of up to ∼3/4 the initial wing area. Noteworthy, insect wings may be damaged by losing surface material without losing wing area. This is due to cracking and tearing of veins and wing membranes, which has recently been reviewed by Rajabi et al. (2020).

As wing damage accumulates over time, the speed of area loss often changes with increasing age of an insect. Several previously published studies found evidence for an increasing rate of damage with increasing time, resulting in an exponential loss in area (Foster and Cartar, 2011; Higginson and Barnard, 2004). However, other authors reported an opposite trend in which wing area loss asymptotically saturates with increasing age. Some of these findings may be explained by the use of an ordinal instead of an interval scale for scoring damage (e.g. Mueller and Wolf-Mueller, 1993; O'Neill et al., 2015). Other authors suggested that a frayed wing tip becomes more compliant and is thus less prone to damage (Mountcastle and Combes, 2014). We observed that in house flies wing damage typically stabilised after an exponential loss. Our logistic function in Fig. 6 combines these two trends, showing an exponential increase at an early stage of wing area loss and an exponential decrease at the late stage. This finding is consistent with (i) the initial increase (∼5% area loss) in honey bees (Higginson and Barnard, 2004), (ii) the assumption that existing damage spreads more easily than initial damage (Foster and Cartar, 2011), and (iii) an increased number of wing collisions owing to changes in wing kinematics and manoeuvrability (Foster and Cartar, 2011). If haemolymph-carrying veins are damaged, wings may even desiccate (Pass et al., 2015; Steppan, 2000; Vincent and Wegst, 2004). Dried wings are more brittle, more stiff, have altered mechanical properties, and should thus exhibit more damage (Hou et al., 2015). As haemolymph circulation also decreases with increasing age of an insect, desiccation is thus a factor that might explain our findings (Arnold, 1964; Salcedo and Socha, 2020).

However, the steepness of wing area loss at t_{tp} (slope) suggests that wing wear in house flies flying in the cylindrical containers is approximately 20 times faster, once begun, than in flies flying inside the larger free-flight cage (Table 1). This result supports the previous assumptions that collisions are the main source of damage to appendages, as suggested for fish (Latremouille, 2003), birds (Francis and Wood, 1989) and several insect species (Burkhard et al., 2002; Foster and Cartar, 2011; O'Neill et al., 2015; Rhainds and Brodersen, 2012). This finding is in line with the difficulties of using wing damage for age grading in wild-caught specimens (Allsopp, 1985; Hayes and Wall, 1999; Lee et al., 2006; Nalepa, 2012; Rhainds and Brodersen, 2012). The cases in which age was successfully derived from wing damage in insects may potentially be explained by flight activity and the number of object collisions (Hargrove, 2020; Hayes et al., 1998; Irvin and Hoddle, 2009; Mueller and Wolf-Mueller, 1993). We have no evidence that our handling procedure and anaesthesia facilitated wing damage.

Wing damage and flight ability

Insects compensate for the loss of wing area by changes in wing kinematics. As already mentioned in the Introduction, pronounced changes include an increase in both wingbeat frequency and amplitude in the damaged wings. If the two wings are differently damaged, amplitude may also decrease in the wing having the larger surface area. Wing damage often attenuates flight performance such as speed (Combes et al., 2010; Fischer and Kutsch, 2000; Haas and Cartar, 2008; Jantzen and Eisner, 2008; Muijres et al., 2017), acceleration and manoeuvrability (Combes et al., 2010; Haas and Cartar, 2008; Mountcastle et al., 2016), and load-lifting capacity (Buchwald and Dudley, 2010; Fernández et al., 2017; Johnson and Cartar, 2014; Roberts and Cartar, 2015). The degree of compensation is limited by several factors, including mechanical

constraints of the wing hinge, maximum frequency of muscle contraction, power output of flight muscles, limits involved in left–right asymmetries, but also by the loss of sensory feedback from the wings (Combes et al., 2010; Lehmann and Dickinson, 1997).

Conventional quasi-steady aerodynamic theory in insect flight links lift production to wing area and characteristic wing velocity. Previous studies suggested maximum lift production in insects of twice the body weight (Lehmann and Dickinson, 1998; Marden, 1987). We thus predicted that an area loss of more than ∼50% should hinder active flight in house flies. Fig. 9C shows that the lower quartile of flight trials corresponds to $\hat{S}$=0.89 (∼10% loss) and the lower whisker to $\hat{S}$=0.76 (∼25% loss). The minimum for an actively flying animal was $\hat{S}$=0.67 (∼33% loss). These data are somewhat below the predicted value but the last of these is similar to the 33% found by Ragland and Sohal (1973) for flying insects. Moreover, our finding is clearly within the range from ∼20% to more than ∼50% area loss that has previously been published for various insect species (Fischer and Kutsch, 2000; Haas and Cartar, 2008; Jantzen and Eisner, 2008; Kassner et al., 2016). As asymmetrical wing area loss may also unbalance aerodynamic force production on the left and right body side (Figs 8C,E,F and 9E,F), flight ability may additionally be attenuated by the induction of turning moments around the yaw, pitch and roll axis of the fly body. Fig. 9E shows that the area difference for 'flying' animals was ∼0.02 median and ∼0.26 maximum for a single fly. In 'non-flying' animals, median area asymmetry was ∼0.40. If flight capacity is mainly constrained by asymmetrical force generation, these differences might reflect the limit that a house fly is able to compensate by neuromuscular-induced changes in wing kinematics such as alterations in wingbeat amplitude, angle of attack, and rotational speed and timing at stroke reversal. We found similar values for the left–right difference in 2nd moment of area with a threshold of 0.4–0.6 between flight and no flight (Fig. 9F). This result is in good agreement with the finding in *Drosophila hydei* that a ∼50% unilateral loss of the wing's 2nd moment of area still allows active flight (Muijres et al., 2017). In house flies, 50% of the 2nd moment of area is 18 $mm^4\,mg^{-1}$, which is close to the lower whisker of the box blot for 'flying' flies (Fig. 9D).

In sum, our study has confirmed previous findings on wing damage and its significance for flight in insects. A missing link between wing damage and flight ability is elaborate data on aerodynamic forces and moments, including the changes in power requirements for flapping damaged wings. This is of ecological interest because previous studies on fish, birds, bats and insects showed that damage to appendages does not necessarily increase energy consumption during locomotion (Fu et al., 2013; Kingsolver, 1999; Voigt, 2013; Webb, 1973). Computer simulations of a phorid fly with unilateral wing damage, for example, showed that total aerodynamic power did not differ much between intact and damaged animals (Lyu et al., 2020). Similar findings have been reported for bumblebee wings. Although wing wear in bumblebees leads to changes in aerodynamic force coefficients and power requirements for flight (induced and profile power), the overall effect was small compared with intact conspecifics (Hedenström et al., 2001). By contrast, flight with moulting wings in humming birds and clipped wings in large moths requires higher metabolic rates than flight with intact wings (Chai, 1997; Fernández et al., 2017). Thus, to further investigate the significance of wing damage in house flies, the presented data are currently being used in a follow-up study to determine the changes in aerodynamic forces, moments and power expenditure in flight with damaged wings using a computational fluid dynamics approach.

Acknowledgements
The authors appreciate help with the experiments and sound analysis algorithm from student intern Evan Grant. We also thank the technicians Bärbel Redlich-Witt, Birgit Wobith and Annegret Mahrwald for their help with fly breeding. Anna Grießbach helped with wing area tracing. H.-N.W. is grateful to Wolf Hanke, Alexander Meister, Sixin Zhang and Kai Schneider for discussions on data analyses. The authors also received helpful input from three anonymous reviewers and appreciate the work put into copy-editing this article.

Competing interests
The authors declare no competing or financial interests.

Author contributions
Conceptualization: H.-N.W., F.-O.L.; Methodology: H.-N.W., T.E., F.-O.L.; Software: H.-N.W., T.E.; Formal analysis: H.-N.W., T.E.; Investigation: H.-N.W.; Resources: T.E.; Writing - original draft: H.-N.W.; Writing - review & editing: F.-O.L.; Visualization: H.-N.W., F.-O.L.; Supervision: F.-O.L.; Project administration: F.-O.L.; Funding acquisition: F.-O.L. (AIFIT, RISE), H.-N. W. (RISE).

Funding
This work was financially supported by the Agence Nationale de la Recherche (ANR, project AIFIT), the Deutsche Forschungsgemeinschaft (DFG, grant LE905/17-1), and the German Academic Exchange Service program RISE (Deutscher Akademischer Austauschdienst) for Evan Grant. The authors were granted access to the HPC resources of TGCC (Très grand centre du calcul du CEA) under the allocation no. 2018-91664 attributed by GENCI (Grand équipement national de calcul intensif).

Data availability
Data are available from the Dryad digital repository (Lehmann, 2021): dryad.t1g1jwt39.

References

Alcock, J. (1996). Male size and survival: the effects of male combat and bird predation in Dawson's burrowing bees, *Amegilla dawsoni*. *Ecol. Entomol.* **21**, 309-316. doi:10.1046/j.1365-2311.1996.00007.x

Allsopp, R. (1985). Wing fray in *Glossina morsitans centralis* Machado (Diptera: Glossinidae). *Bull. Entomol. Res.* **75**, 1-11. doi:10.1017/S0007485300014127

Anderson, K. E. and Keyel, A. C. (2006). Mating flight, metrosis, and semi-claustrality in the seed-harvester ant *Pogonomyrmex salinus* (Hymenoptera, Formicidae). *Insectes Soc.* **53**, 92-96. doi:10.1007/s00040-005-0840-y

Arnold, J. W. (1964). Blood circulation in insect wings. *Memoirs Entomol. Soc. Can.* **96**, 5-60. doi:10.4039/entm9638fv

Benson, W. W. (1972). Natural selection for Müllerian mimicry in *Heliconius erato* in Costa Rica. *Science* **176**, 936-939. doi:10.1126/science.176.4037.936

Buchwald, R. and Dudley, R. (2010). Limits to vertical force and power production in bumblebees (Hymenoptera: *Bombus impatiens*). *J. Exp. Biol.* **213**, 426-432. doi:10.1242/jeb.033563

Burkhard, D. U., Ward, P. I. and Blanckenhorn, W. U. (2002). Using age grading by wing injuries to estimate size-dependent adult survivorship in the field: a case study of the yellow dung fly *Scathophaga stercoraria*. *Ecol. Entomol.* **27**, 514-520. doi:10.1046/j.1365-2311.2002.00453.x

Cartar, R. V. (1992). Morphological senescence and longevity: an experiment relating wing wear and life span in foraging wild bumble bees. *J. Anim. Ecol.* **61**, 225-231. doi:10.2307/5525

Casey, T. M. and Ellington, C. P. (1989). Energetics of insect flight. In *Energy Transformations in Cells and Organisms* (ed. W. Wieser and E. Gnaiger), pp. 200-210. Stuttgart: Thieme.

Chai, P. (1997). Hummingbird hovering energetics during moult of primary flight feathers. *J. Exp. Biol.* **200**, 1527-1536. doi:10.1242/jeb.200.10.1527

Combes, S. A., Crall, J. D. and Mukherjee, S. (2010). Dynamics of animal movement in an ecological context: dragonfly wing damage reduces flight performance and predation success. *Biol. Lett.* **6**, 426-429. doi:10.1098/rsbl.2009.0915

Danzer, A. (1956). Der Flugapparat der Dipteren als Resonanzsystem. *Z. Vgl. Physiol.* **38**, 259-283. doi:10.1007/BF00341301

Davies, N. B. (1978). Territorial defence in the speckled wood butterfly (*Pararge aegeria*): the resident always wins. *Anim. Behav.* **26**, 138-147. doi:10.1016/0003-3472(78)90013-1

Dukas, R. and Dukas, L. (2011). Coping with nonrepairable body damage: effects of wing damage on foraging performance in bees. *Anim. Behav.* **81**, 635-638. doi:10.1016/j.anbehav.2010.12.011

Ellington, C. P. (1984). The aerodynamics of hovering insect flight. I. The quasi-steady analysis. *Philos. Trans. R. Soc. Lond. B* **305**, 1-15. doi:10.1098/rstb.1984.0049

Fernández, M. J., Springthorpe, D. and Hedrick, T. L. (2012). Neuromuscular and biomechanical compensation for wing asymmetry in insect hovering flight. *J. Exp. Biol.* **215**, 3631-3638. doi:10.1242/jeb.073627
Fernández, M. J., Driver, M. E. and Hedrick, T. L. (2017). Asymmetry costs: effects of wing damage on hovering flight performance in the hawkmoth *Manduca sexta*. *J. Exp. Biol.* **220**, 3649-3656. doi:10.1242/jeb.153494
Fischer, H. and Kutsch, W. (2000). Relationships between body mass, motor output and flight variables during free flight of juvenile and mature adult locusts, *Schistocerca gregaria*. *J. Exp. Biol.* **203**, 2723-2735. doi:10.1242/jeb.203.18.2723
Foster, D. J. and Cartar, R. V. (2011). What causes wing wear in foraging bumble bees? *J. Exp. Biol.* **214**, 1896-1901. doi:10.1242/jeb.051730
Francis, C. M. and Wood, D. S. (1989). Effects of age and wear on wing length of wood-warblers (Efecto de la edad y el desgaste en el largo del ala de Emberísidos (Emberizidae)). *J. Field Ornithol.* **60**, 495-503.
Fu, C., Cao, Z.-D. and Fu, S.-J. (2013). The effects of caudal fin amputation on metabolic interaction between digestion and locomotion in juveniles of three cyprinid fish species with different metabolic modes. *Comp. Biochem. Physiol. A* **164**, 456-465. doi:10.1016/j.cbpa.2012.12.015
Haas, C. A. and Cartar, R. V. (2008). Robust flight performance of bumble bees with artificially induced wing wear. *Can. J. Zool.* **86**, 668-675. doi:10.1139/Z08-034
Hargrove, J. W. (1975). The flight performance of tsetse flies. *J. Insect Physiol.* **21**, 1385-1395. doi:10.1016/0022-1910(75)90264-4
Hargrove, J. W. (2020). A model for the relationship between wing fray and chronological and ovarian ages in tsetse (*Glossina* spp). *Med. Vet. Entomol.* **34**, 251-263. doi:10.1111/mve.12439
Hayes, E. J. and Wall, R. (1999). Age-grading adult insects: a review of techniques. *Physiol. Entomol.* **24**, 1-10. doi:10.1046/j.1365-3032.1999.00104.x
Hayes, E. J., Wall, R. and Smith, K. E. (1998). Measurement of age and population age structure in the blowfly, *Lucilia sericata* (Meigen) (Diptera: Calliphoridae). *J. Insect Physiol.* **44**, 895-901. doi:10.1016/S0022-1910(98)00067-5
Hedenström, A., Ellington, C. P. and Wolf, T. J. (2001). Wing wear, aerodynamics and flight energetics in bumblebees (*Bombus terrestris*): an experimental study. *Funct. Ecol.* **15**, 417-422. doi:10.1046/j.0269-8463.2001.00531.x
Higginson, A. D. and Barnard, C. J. (2004). Accumulating wing damage affects foraging decisions in honeybees (*Apis mellifera* L.). *Ecol. Entomol.* **29**, 52-59. doi:10.1111/j.0307-6946.2004.00573.x
Higginson, A. D. and Gilbert, F. (2004). Paying for nectar with wingbeats: a new model of honeybee foraging. *Proc. Roy. Soc. Lond. B* **271**, 2595-2603. doi:10.1098/rspb.2004.2866
Higginson, A. D., Barnard, C. J., Tofilski, A., Medina, L. and Ratnieks, F. (2011). Experimental wing damage affects foraging effort and foraging distance in honeybees *Apis mellifera*. *Psyche* **2011**, 419793. doi:10.1155/2011/419793
Hou, D., Yin, Y., Zhao, H. and Zhong, Z. (2015). Effects of blood in veins of dragonfly wing on the vibration characteristics. *Comp. Biol. Med.* **58**, 14-19. doi:10.1016/j.compbiomed.2014.12.018
Irvin, N. A. and Hoddle, M. S. (2009). Egg maturation, oosorption, and wing wear in *Gonatocerus shmeadi* (Hymenoptera: Mymaridae), an egg parasitoid of the glassy-winged sharpshooter, Homalodisca vitripennis (Hemiptera: Cicadellidae). *Biol. Control* **48**, 125-132. doi:10.1016/j.biocontrol.2008.10.013
Jantzen, B. and Eisner, T. (2008). Hindwings are unnecessary for flight but essential for execution of normal evasive flight in Lepidoptera. *Proc. Natl. Acad. Sci. USA* **105**, 16636-16640. doi:10.1073/pnas.0807223105
Johnson, S. A. and Cartar, R. V. (2014). Wing wear, but not asymmetry in wear, affects load-lifting capability in bumble bees *Bombus impatiens*. *Can. J. Zool.* **92**, 179-184. doi:10.1139/cjz-2013-0229
Kammerer, P. (1907). Regeneration des Dipterenflügels beim Imago. *Arch. Entwicklunsmech. Organ.* **25**, 349-360. doi:10.1007/BF02292171
Kassner, Z., Dafni, E. and Ribak, G. (2016). Kinematic compensation for wing loss in flying damselflies. *J. Insect Physiol.* **85**, 1-9. doi:10.1016/j.jinsphys.2015.11.009
Kingsolver, J. G. (1999). Experimental analyses of wing size, flight, and survival in the western white butterfly. *Evolution* **53**, 1479-1490. doi:10.1111/j.1558-5646.1999.tb05412.x
Kiritani, K., Yamashita, H. and Yamamura, K. (2013). Beak marks on butterfly wings with special reference to Japanese black swallowtail. *Popul. Ecol.* **55**, 451-459. doi:10.1007/s10144-013-0375-4
Kříženecký, J. (1914). Experimentelle und theoretische Untersuchungen über die Restitution der Insektenflügel. *Arch. Entwicklunsmech. Organ.* **39**, 177-216. doi:10.1007/BF02267087
Lane, S. J., Frankino, W. A., Elekonich, M. M. and Roberts, S. P. (2014). The effects of age and lifetime flight behavior on flight capacity in *Drosophila melanogaster*. *J. Exp. Biol.* **217**, 1437-1443. doi:10.1242/jeb.095646
Latremouille, D. N. (2003). Fin erosion in aquaculture and natural environments. *Rev. Fish. Sci.* **11**, 315-335. doi:10.1080/10641260390255745
Lee, J. C., Leibee, G. L. and Heimpel, G. E. (2006). Broken wing fringe setae as a relative estimate of parasitoid age. *Entomol. Exp. Appl.* **121**, 87-92. doi:10.1111/j.1570-8703.2006.00446.x
Lehmann, F.-O. (2021). Flight activity and age cause wing damage in house flies, Dryad, Dataset. https://doi.org/10.5061/dryad.t1g1jwt39.
Lehmann, F.-O. and Dickinson, M. H. (1997). The changes in power requirements and muscle efficiency during elevated force production in the fruit fly, *Drosophila melanogaster*. *J. Exp. Biol.* **200**, 1133-1143. doi:10.1242/jeb.200.7.1133
Lehmann, F.-O. and Dickinson, M. H. (1998). The control of wing kinematics and flight forces in fruit flies (*Drosophila* spp.). *J. Exp. Biol.* **201**, 385-401. doi:10.1242/jeb.201.3.385
Lyu, Y. Z., Zhu, H. J. and Sun, M. (2020). Wing kinematic and aerodynamic compensations for unilateral wing damage in a small phorid fly. *Phys. Rev. E* **101**, 012412. doi:10.1103/PhysRevE.101.012412
Marden, J. H. (1987). Maximum lift production during takeoff in flying animals. *J. Exp. Biol.* **130**, 235-258. doi:10.1242/jeb.130.1.235
Monge-Nájera, J., Hernández, F., Gonzáles, M. I., Soley, J., Araya, J. and Zolla, S. (1998). Spatial distribution, territoriality and sound production by tropical cryptic butterflies (*Hamadryas*, Lepidoptera: Nymphalidae): implications for the "industrial melanism" debate. *Rev. Biol. Trop.* **46**, 297-330. doi:10.15517/rbt.v46i2.19532
Mountcastle, A. M. and Combes, S. A. (2014). Biomechanical strategies for mitigating collision damage in insect wings: structural design versus embedded elastic materials. *J. Exp. Biol.* **217**, 1108-1115. doi:10.1242/jeb.092916
Mountcastle, A. M., Alexander, T. M., Switzer, C. M. and Combes, S. A. (2016). Wing wear reduces bumblebee flight performance in a dynamic obstacle course. *Biol. Lett.* **12**, 20160294. doi:10.1098/rsbl.2016.0294
Mueller, U. G. and Wolf-Mueller, B. (1993). A method for estimating the age of bees: age-dependent wing wear and coloration in the wool-carder bee *Anthidium manicatum* (Hymenoptera: Megachilidae). *J. Insect Behav.* **6**, 529-537. doi:10.1007/BF01049530
Muijres, F. T., Iwasaki, N. A., Elzinga, M. J., Melis, J. M. and Dickinson, M. H. (2017). Flies compensate for unilateral wing damage through modular adjustments of wing and body kinematics. *Interface Focus* **7**, 20160103. doi:10.1098/rsfs.2016.0103
Nalepa, C. A. (2012). Wing wear is a poor estimate of age in *Cerceris fumipennis* (Hymenoptera, Crabronidae). *J. Hymenopt. Res.* **24**, 43-46. doi:10.3897/jhr.24.2091
O'Neill, K. M., Delphia, C. M. and Pitts-Singer, T. L. (2015). Seasonal trends in the condition of nesting females of a solitary bee: wing wear, lipid content, and oocyte size. *PeerJ* **3**, e930. doi:10.7717/peerj.930
Pass, G., Tögel, M., Krenn, H. and Paululat, A. (2015). The circulatory organs of insect wings: prime examples for the origin of evolutionary novelties. *Zool. Anzeiger* **256**, 82-95. doi:10.1016/j.jcz.2015.03.008
Pinheiro, C. E. G. (1990). Territorial hilltopping behavior of three swallowtail butterflies (Lepidoptera, Papilionidae) in Western Brazil. *J. Res. Lepid.* **29**, 134-142.
Ragland, S. S. and Sohal, R. S. (1973). Mating behavior, physical activity and aging in the housefly, *Musca domestica*. *Exp. Gerontol.* **8**, 135-145. doi:10.1016/0531-5565(73)90003-X
Ragland, S. S. and Sohal, R. S. (1975). Ambient temperature, physical activity and aging in the housefly, *Musca domestica*. *Exp. Gerontol.* **10**, 279-289. doi:10.1016/0531-5565(75)90005-4
Rajabi, H., Schroeter, V., Eshghi, S. and Gorb, S. N. (2017). The probability of wing damage in the dragonfly *Sympetrum vulgatum* (Anisoptera: Libellulidae): a field study. *Biol. Open* **6**, 1290-1293. doi:10.1242/bio.027078
Rajabi, H., Dirks, J.-H. and Gorb, S. N. (2020). Insect wing damage: causes, consequences and compensatory mechanisms. *J. Exp. Biol.* **223**, jeb215194. doi:10.1242/jeb.215194
Rehan, S. M. and Richards, M. H. (2010). The influence of maternal quality on brood sex allocation in the small carpenter bee, *Ceratina calcarata*. *Ethology* **116**, 876-887. doi:10.1111/j.1439-0310.2010.01804.x
Rhainds, M. and Brodersen, G. (2012). Wing wear of adult *Choristoneura fumiferana* (Lepidoptera: Tortricidae) in relation to age, sex, sex ratio, and presence of host plant. *Appl. Entomol. Zool.* **47**, 475-478. doi:10.1007/s13355-012-0137-3
Roberts, J. C. and Cartar, R. V. (2015). Shape of wing wear fails to affect load lifting in common eastern bumble bees (*Bombus impatiens*) with experimental wing wear. *Can. J. Zool.* **93**, 531-537. doi:10.1139/cjz-2014-0317
Salcedo, M. K. and Socha, J. J. (2020). Circulation in insect wings. *Integr. Comp. Biol.,* **60**, 1208-1220. doi:10.1093/icb/icaa124
Schindelin, J., Arganda-Carreras, I., Frise, E., Kaynig, V., Longair, M., Pietzsch, T., Preibisch, S., Rueden, C., Saalfeld, S., Schmid, B. et al. (2012). Fiji: an open-source platform for biological-image analysis. *Nat. Meth.* **9**, 676-682. doi:10.1038/nmeth.2019
Skovgård, H., Nachman, G. (2004). Biological control of house flies *Musca domestica* and stable flies *Stomoxys calcitrans* (Diptera: Muscidae) by means of inundative releases of *Spalangia cameroni* (Hymenoptera: Pteromalidae). *Bull. Entomol. Res.* **94**, 555-567. doi:10.1079/BER2004322
Sohal, R. S. and Buchan, P. B. (1981). Relationship between physical activity and life span in the adult housefly, *Musca domestica*. *Exp. Gerontol.* **16**, 157-162. doi:10.1016/0531-5565(81)90040-1
Sotavalta, O. (1952a). *The Essential Factor Regulating the Wing-Stroke Frequency of Insects in Wing Mutilation and Loading Experiments and in Experiments at*

Subatmospheric Pressure, 15. Suomalaisen Eläin- ja Kasvitieteellisen Seuran Vanamon Eläintieteellisiä Julkaisuja.

Sotavalta, O. (1952*b*). Flight-tone and wing-stroke frequency of insects and the dynamics of insect flight. *Nature* **170**, 1057-1058. doi:10.1038/1701057a0

Steppan, S. J. (2000). Flexural stiffness patterns of butterfly wings (Papilionoidea). *J. Res. Lepidoptera,* **35**, 61-77.

Vance, J. T. (2009). Experimental and natural variation in hovering flight capacity in bees, Hymenoptera: Apidae. *UNLV Theses, Dissertations, Professional Papers, and Capstones*, Vol. 26: Digital Scholarship@UNLV.

Vance, J. T. and Roberts, S. P. (2014). The effects of artificial wing wear on the flight capacity of the honey bee *Apis mellifera*. *J. Insect Physiol.* **65**, 27-36. doi:10.1016/j.jinsphys.2014.04.003

Vincent, J. F. V. and Wegst, U. G. K. (2004). Design and mechanical properties of insect cuticle. *Arthropod Struct. Dev.* **33**, 187-199. doi:10.1016/j.asd.2004.05.006

Voigt, C. C. (2013). Bat flight with bad wings: is flight metabolism affected by damaged wings? *J. Exp. Biol.* **216**, 1516-1521. doi:10.1242/jeb.079509

Webb, P. W. (1973). Effects of partial caudal-fin amputation on the kinematics and metabolic rate of underyearling sockeye salmon (*Oncorhynchus nerka*) at steady swimming speeds. *J. Exp. Biol.* **59**, 565-582. doi:10.1242/jeb.59.3.565

Weis-Fogh, T. (1973). Quick estimates of flight fitness in hovering animals, including novel mechanisms for lift production. *J. Exp. Biol.* **59**, 169-230. doi:10.1242/jeb.59.1.169

Werber, I. (1907). Regeneration der exstirpierten Flügel beim Mehlkäfer (*Tenebrio molitor*). *Arch. Entwicklunsmech. Organ.* **25**, 344-348. doi:10.1007/BF02292170

Werber, I. (1911). Über regeneratähnliche Flügelmißbildung einer Stubenfliege (*Musca domestica* L). *Zool. Anz.* **37**, 1-7.

Wilson, D. M. and Weis-Fogh, T. (1962). Patterned activity of co-ordinated motor units, studied in flying locusts. *J. Exp. Biol.,* **39**, 643-667. doi:10.1242/jeb.39.4.643

Supplementary Materials and Methods 1

Temperature and relative humidity

Measurements during the experiment

For the experiment, we used a logger (BL-30, Trotec GmbH, Heinsberg, Germany) that measured temperature and relative humidity of the ambient air. In the container experiments, it was placed close to the containers. Control measurements, however, revealed that the measured relative humidity and temperature of the room is the lower boundary of the values inside the containers: internal relative humidity was ~75% due to the water supply. Assuming that mean temperature inside the vials was 2 °C higher than the measured room temperature during the day (due to the lamps) and identical during the night, and assuming a lifetime of 60 days, this converts into 60 Kd (7%) offset of physiological age for temperatures ca. 15 °C above the threshold (i.e. ca. 26 °C). For the free-flight experiment, the values measured next to the cage corresponds well to the values inside the cage for both humidity and temperature. Temperature and illuminance were also measured outdoors and inside the setups to allow further comparisons. Temperature, relative humidity and illuminance was 24.7±2.8 °C, 38±6% and 380-840 lx in container experiments and 24.1±0.8 °C, 41±7% and 350-42000 lx in free flight experiments, respectively. Measurements outside were done on days with temperatures between 19 °C and 26 °C and illuminances between 6000 lx and 120 000 lx.

Estimation of the physiological age

Temperature influences the activity and metabolism of a fly. We thus used physiological age (Skovgård and Nachman, 2004) instead of age. Temperature was recorded during 63-73% of the experimental time. To continuously estimate physiological age, we thus derived temperature means for each light and dark period and interpolated missing data using weighted linear regression (Fig. S1). In containers, this interpolation assumed t_0=0 min on midnight (00:00:00) on July 21th, 2018 (activity experiment), and midnight (00:00:00) on April 20th, 2018 (free-flight experiment). For container experiments, the linear equations was $T(t)=at+b$ (with a = -2.617×10^{-3} °Ch^{-1} and b = 29.87 °C for day temperatures; adjusted R^2 = 0.911; and a = -2.373×10^{-3} °Ch^{-1} and b = 28.79 °C for night temperatures; adjusted R^2 = 0.942). In flight cage experiments, the coefficients were a = 0.1002×10^{-3} °Ch^{-1} and b = 24.52 °C for day temperatures (adjusted R^2 = -0.0145), and a = 0.2453×10^{-3} °Ch^{-1} and b = 23.34 °C for night temperatures (adjusted R^2 = 0.0006). For the temperature integral, we used our estimated means for each light/dark cycle and for physiological age estimation a reference temperature of 11 °C (Skovgård and Nachman, 2004). Figure S2A, B shows the relationship between chronological and physiological age for all tested flies. In the container experiment, different cohorts were started at different times as shown by different colours. In flight experiment, we tested only one cohort of flies. Survivorship plots for both age measures are shown for container experiment in figure S2C-F and for flight experiment in figure S2G, H.

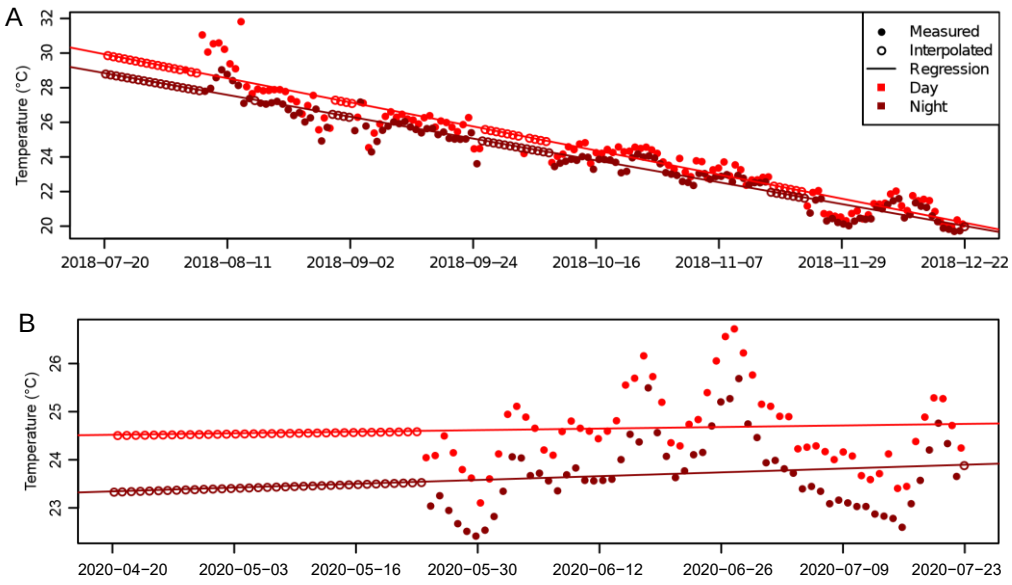

Fig. S1. Measured (filled circles) and interpolated/extrapolated (open circles) temperature data for each day (light red) and night (dark red) section for (A) container and (B) flight cage experiments. Lines, linear regression fit. X-scale shows date.

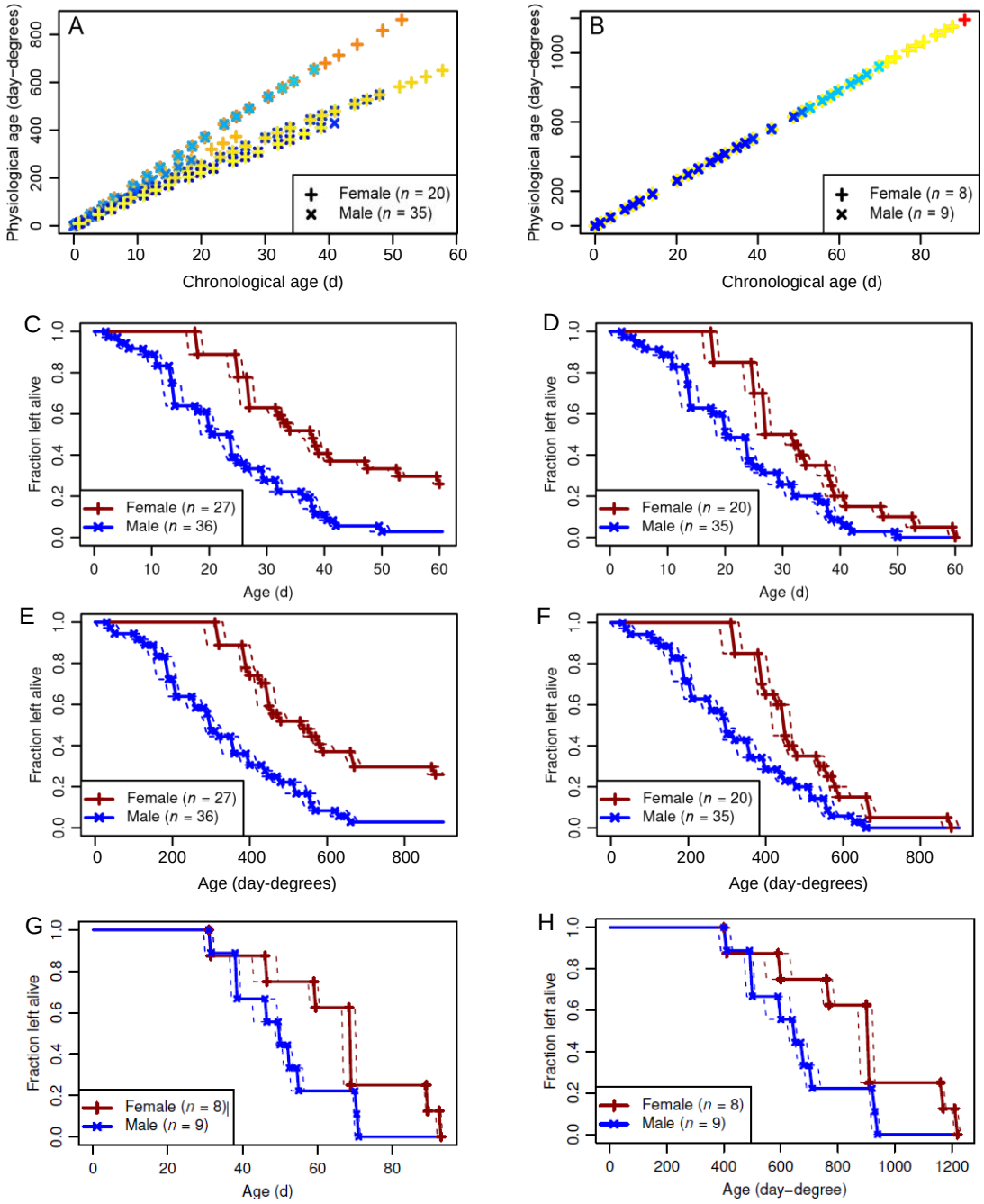

Fig. S2. Age comparison and mortality. (A, B) Physiological compared to chronological age for container in *A* and flight cage experiments in *B*. We tested several groups (cohorts), thus data overlap (see text S1). (C-F) Mortality of flies in container experiment for chronological age in *C* and *D*, and physiological age in *E* and *F*. *C*, *E*: all experimental flies; *D*, *F*: only those that died during the experimental time (and could therefore be entered into the analysis). Dashed lines show minimum and maximum values. Solid lines indicate means. (G, H) Mortality of flies used in free flight experiment for chronological age in *G* and physiological age in *H*. Dashed lines show minimum and maximum values, solid lines means.

Supplementary Materials and Methods 2

Software

The software used for data analyses and processing is shown in Table S1.

Table S1. List of software used in this study.

Software	Used for	URL/Reference
Fiji	image mask creation	Schindelin et al. (2012)
ffmpeg	video processing	https://ffmpeg.org
ImageMagick	image processing	https://imagemagick.org
MediaHuman	audio resampling	https://mediahuman.com
processing	image analysis	https://processing.org
Python 3.x	sound analysis, image	https://python.org
R	data processing, analysis	https://www.r-project.org R Core Team (2020)
RStudio	GUI for R	https://rstudio.com
R packages		
abind	array manipulation	Plate and Heiberger (2016)
colorRamps	template for colour tables	Keitt (2012)
data.table	data manipulation	Dowle and Srinivasan (2019)
extrafont	using system fonts	Chang (2014)
exifr	extracting EXIF data	Dunnington and Harvey (2019)
imager	image processing	Barthelme (2020)
jpeg	image processing	Urbanek (2019)
lattice	data visualisation	Sarkar (2008)
magick	image processing	Ooms (2020)
minpack.lm	fitting arbitrary functions	Elzhov et al. (2016)
png	image processing	Urbanek (2013a)
rChoiceDialogs	file explorer	Lisovich and Day (2014)
rcompanion	histogram plotting	Mangiafico (2020)
smoothSurv	basis for piecewise functions	Komárek et al. (2005)
stringi	unicode characters	Gagolewski (2020)
tiff	image processing	Urbanek (2013b)
tuneR	sound analysis	Ligges et al. (2018)

Supplementary Materials and Methods 3

Flight activity in container

Validation of flight activity

To validate our software that was developed to detect flight events in the containers, we conducted a control experiment, in which flight was simultaneously filmed by a Nikon D7100 (Tokyo, Japan) and sound recorded by a Tascam-US-16x08 filter unit (TEAC Europe). Filter settings for gain, frequency, and if applicable Q-factor was -12 dB and 1.7 kHz for high range; 9 dB, 450 Hz, and 0.25 for high mid range; and 12 dB, 350 Hz, and 0.25 for low mid range, respectively. In each control experiment, we placed 5-day old flies into a container in groups of four and filmed their activity for 30 minutes. We tested 3 female and 3 male groups. Temperature inside the container varied between 26.3 °C and 28.6 °C. The software algorithm identified 1395 flight bouts, 507 (~36 %) were manually inspected, of which 85 were dismissed. We found that during bouts corresponding to a total of 144 video frames flies did not fly and in bouts corresponding to 2652 frames at least one flying fly. False-positive rate was ~6 %. In ~41 % of the cases, in which the sound software falsely identified flight bouts, a fly was close to the microphone.

Eventually, from the manually inspected bouts, we further scored 153 “flight bouts” from parts of the video where the algorithm had not identified flight activity. These correspond to 6182 video frames. Never was a fly observed to be flying during these bouts. Sometimes flies beat their wings without (any fly) flying, giving an approximate false negative rate of finding purely sitting activity of less than 1 %. We found that most of the time,

only one fly was active at a time (2428 frames). In ~3.6% of the frames two flies were active (224 frames) that apparently stimulated each other (Fig. S3). We also estimated the likelihood of one active fly by random model and compared these data to the recorded signals and from this decided to assume that on overage only one fly is active at any one time during any sound-recorded flight bout.

Supplementary Materials and Methods 4

Validation of wing outline tracing

Wing outline tracing was manually done by hand using a graphics tablet. This approach yielded maximum errors in wing area of ~1.1% when traced by different persons with a median of ~-0.4% (N=33 traced wing outlines), respectively. Having the same person tracing one wing twice resulted in a difference in wing area of about 0.5%. Automatic tracking procedures were not capable of reliably detecting wing shape and orientation.

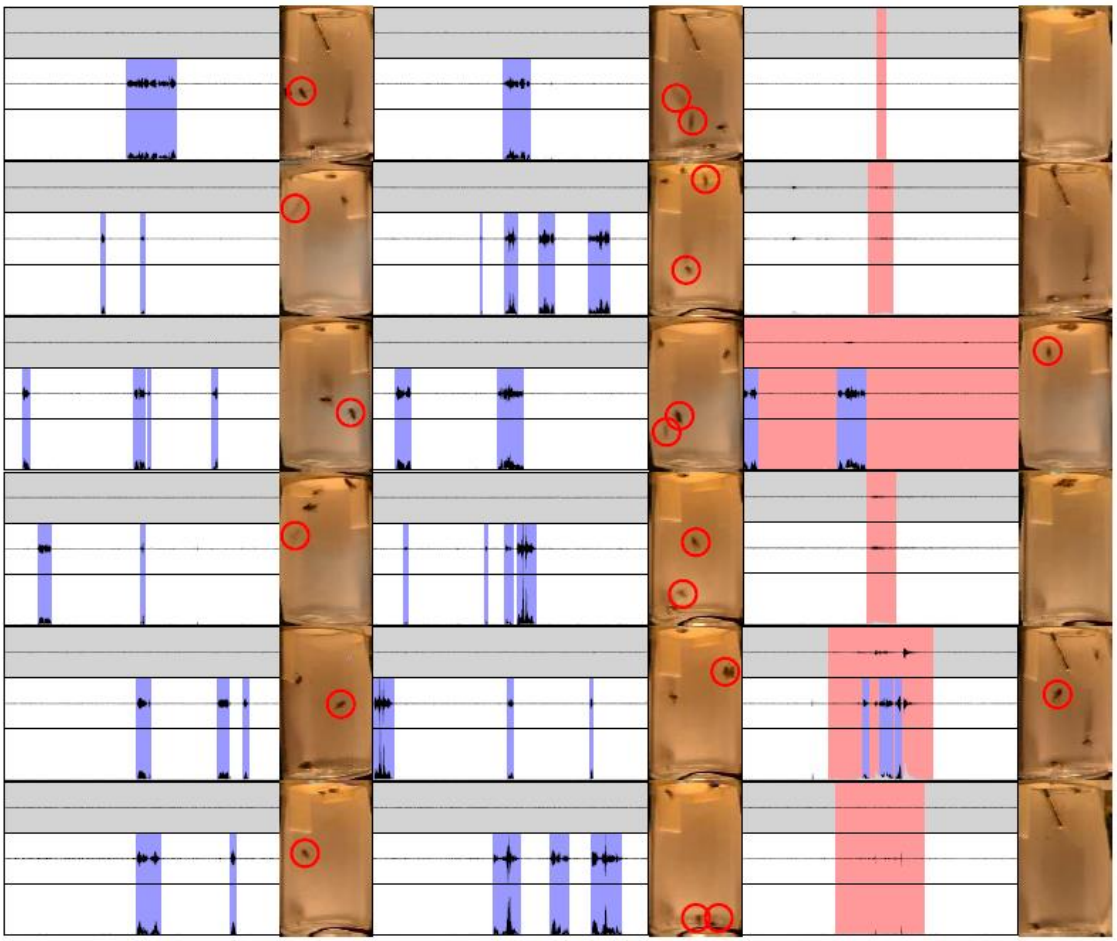

Fig. S3. Validation of flight bout recognition by sound recording. Each example shows five seconds of flight and consists of three horizontal traces and a corresponding photo to the right. The upper trace (background shaded in grey) is the sound signal of the room tone microphone, and the middle trace the sound signal of the microphone of the container. The lower trace shows the bandpass-filtered sound signal. Blue shaded areas indicate flight bouts as found by the sound software. Red shaded areas show an example in which there is external noise not recognised as flight. Red circles in each container indicate flying flies.

Supplementary Materials and Methods 5

Reconstruction of wing root area

The reference wing area is shown in red in figure S4A. We made no attempt to measure the area close to the wing root (P1-P3, Fig. 1B) because this part of the wing mostly stayed intact. Wings were aligned by superimposing the point at the humeral cross-vein (red cross with circle in Fig S4A) and rotating the wing around this point until the crossing between anal vein A_2 and cubitus A_1+CuA_2 was vertically aligned with the pivoting

Journal of Experimental Biology • Supplementary information

point (nomenclature as in McAlpine, 1981). Vein crossings were manually assigned and wing rotation was done using a script written in *R*. A *Python* script turned all wings further around the pivoting point at the humeral cross-vein so as to find the maximum area overlap.

For calculation of moments of wing area, we determined the wings' longitudinal axis. A mean wing root position per experiment and sex was calculated from the initial wing photos. Similarly, a mean direction from root to tip was calculated. These mean values were used for all wings and the tip direction was assumed to stay constant throughout the experiment, even for cases where wing areas were missing. Root position and tip direction (x,y; video pixel) in container experiments was (2368,213)±(15,10), (−0.9858,0.1680)±(0.0031,0.0171) in females, and (2350,211)±(15,9) and (−0.9866,0.1632)±(0.0026,0.0157) in males. In free-flight experiments it was (4629,386)±(15,13) and (−0.9799,0.1995)±(0.0025,0.0121) in females, and (4620,395)±(14,12) and (−0.9822,0.1878)±(0.0029,0.0148) in males. As the area at the wing root (P1-P3, red, Fig. 1A, main text) was not measured, but may influence the value of the second moment of area especially for strongly damaged wings, we added an average "wing root dummy" to the measured wing outline for calculating the area moments. We compared values of area moments between wing outlines without a root dummy (see fig. S4D) and with two different root dummies (a polygon based on the tracked points used for aligning the wings, fig. S4E; and an average wing root -- excluding the alula -- roughly estimated from five photos for each sex in both container and free-flight experiment separately, fig. S4F). As the difference between the two types of dummy was small, we opted for the average traced wing root.

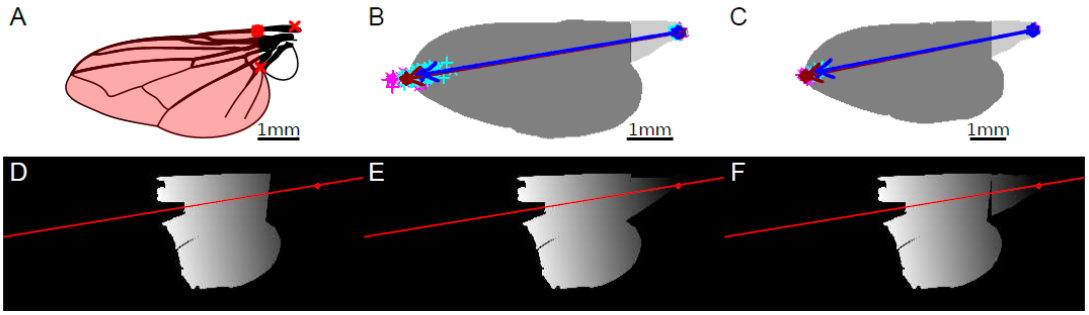

Fig. S4. (A) Schematics showing the traced wing area (red) and points used for alignment of all wings (red crosses). (B,C) Example wing mask (dark grey) with attached standard root (light grey), wing tip and root positions (magenta: single female, dark red: mean female, cyan: single male, blue: mean male) and vectors (longitudinal wing axis) from mean root to mean tip. Drawing in *B* applies to container experiment and in *C* to free-flight experiments in the large flight cage. (D-F) Calculation of the second moment of wing area for a damaged left wing mask of a male fly from the container experiment with mean wing root (red dot) and direction towards wing tip (red line). *D*, traced area only; *E*, polygon root area; *F*, mean root area.

Supplementary Materials and Methods 6

Derivation of equations for A_k and S_k

This section shows how we calculated the 2nd moment of area for one wing from Ellington's (Ellington, 1984b) theoretical framework on two wings. Ellington defined wing area as the total area of both wings:

$$S_{Ellington} = 2\int_0^R c\,d\hat{r}\,, \qquad \text{(eq. S1)}$$

with R the wing length of one wing, $0 \le r \le R$ the position along the wing, and $c(r)$ the wing chord at position r. Area of a single wing is thus:

$$A = \int_0^R c\,dr = \frac{S_{Ellington}}{2} \qquad \text{(eq. S2)}$$

The wings' aspect ratio as introduced by Ellington is defined for both wings as:

$$AR_{Ellington} = \frac{2R}{\bar{c}} = \frac{4R^2}{S_{Ellington}}\,, \qquad \text{(eq. S3)}$$

with mean wing chord:

$$\bar{c} = \frac{A}{R} = \frac{S_{Ellington}}{2R} \qquad \text{(eq. S4)}$$

For a single wing equation S4 may be written as:

$$AR = \frac{R}{\bar{c}} = \frac{R^2}{A} = \frac{AR_{Ellington}}{2} . \quad \text{(eq. S5)}$$

Replacing wing length and chord by their relative expressions $\hat{r} = r/R$ and $\hat{c} = c/\bar{c}$, the *k*-th moment of wing area is:

$$\begin{aligned} S_{k,Ellington} &= 2\int_0^R cr^k dr \quad \text{(eq. S6)} \\ &= 2\int_0^R \hat{c}\bar{c}(\hat{r}R)^k dr \\ &= 2\int_0^R \bar{c}R^k \hat{c}\hat{r}^k dr \\ &= 2\int_0^R \frac{S_{Ellington}}{2R} R^k \hat{c}\hat{r}^k dr \\ &= S_{Ellington}R^k \int_0^R \hat{c}\hat{r}^k R^{-1} dr . \end{aligned}$$

Considering integration bounds, this equation converts into:

$$S_{k,Ellington} = S_{Ellington}R^k \int_0^1 \hat{c}\hat{r}^k dr . \quad \text{(eq. S7)}$$

The latter equation derives integrated wing area to the power of *k* for each wing blade element along the position *r*. Assuming symmetrical wings on both sides of the animal, we may write the *k*-th moment of area of a single wing as:

$$A_k = \int_0^R cr^k dr = AR^k \int_0^1 \hat{c}\hat{r}^k d\hat{r} = \frac{S_{k,Ellington}}{2} . \quad \text{(eq. S8)}$$

However, due to wing damage, there is no symmetry between left and right wing. This requires to calculate $S = A_L + A_R$ and $S_k = A_{k,L} + A_{k,R}$ with L and R the left and right wing, respectively. Aspect ratio (AR) is thus:

$$AR_{total} = \frac{(R_L + R_R)^2}{A_L + A_R} = \frac{(R_L + R_R)^2}{S} . \quad \text{(eq. S9)}$$

Noteworthy, this approach ignores the body between both wings. Ellington's expression of the non-dimensional *k*-th moment $\hat{r}_k^k$ is equal to:

$$\hat{r}^k_{k,Ellington}(S_{Ellington}) = \frac{S_{k,Ellington}}{S_{Ellington}R^k} = \int_0^1 \hat{c}\hat{r}^k d\hat{r} . \quad \text{(eq. S10)}$$

For a single wing this expression should be written as:

$$\hat{r}_k^k(A) = \frac{A_k}{A \cdot R^k} \int_0^1 \hat{c}\hat{r}^k d\hat{r} = \hat{r}^k_{k,Ellington}(S_{Ellington}) , \quad \text{(eq. S11)}$$

that is identical to Ellington because $\hat{r}_k^k$ is area-independent. The last step is to calculate the non-dimensional radius of the *k*-th moment of wing area, $\hat{r}_k$. According to Ellington, the *k*-th moment of area would be S_k, and the characteristics of the wing planform $\hat{r}_k$ is:

$$\hat{r}_k = \sqrt[k]{\hat{r}_k^k} . \quad \text{(eq. S12)}$$

Supplementary Materials and Methods 7

Similarity of wing damage progression within containers

In the container experiment, flies were kept in groups of four animals and an averaged activity was assigned to each fly. This approach may result in wing damage progression that is more similar in flies from the same group compared to flies from another groups. If flies within a single container are more similar to each other than to other flies, the variance in number of damaged wings, ages at t_{tp}, and logistic fit parameters should be different from randomly assigned pairings. We approached this problem by creating an elevated number of random permutations, shuffling around the flies' group memberships. We tested up to 999 artificial permutations and compared data from the mixed memberships with the data from the measured memberships. For each permutation, we estimated the fraction of damaged wings for all flies with an area loss of more than 15%. A similar procedure we applied to maximum-minimum range of physiological age and logistic parameters (Fig. S5A-H).

To compare the fraction of damaged wings in measured groups with permutated groups, we used a two-sided two-sample Kolmogorov-Smirnov test. We assigned a number to each fly container and ranked them according to the span of ages the flies of each group permutation reached (Fig. S5I). The relative position of the real group was determined. In case of ties, the real group was considered to be in the middle of the tied permutations. If membership does not matter, the ranks should scatter around 0.5. Relative rank was tested by a one-sided *t*-tests on its equality with 0.5 (alternative hypothesis: <0.5). Probability values of Kolmogorov-Smirnov and *t*-tests were also corrected for multiple measurements using Bonferroni correction. In none of the tests, we found any significance between differently grouped memberships (*p*-values for females: 1.00 for fraction of damaged wings, 0.566 for age; males: 1.00 for fraction of damaged wings, 0.168 for age). Data for permutations of logistic fit parameters (analysed in a manner similar to that of age; ranks pooled across parameters of the fits) is shown in figure S5I, J. While medians and arithmetic means were below 0.5 for males, none of the tests showed statistical difference from 0.5. Altogether, the results suggest that group membership has no significance for wing damage patterns in our study.

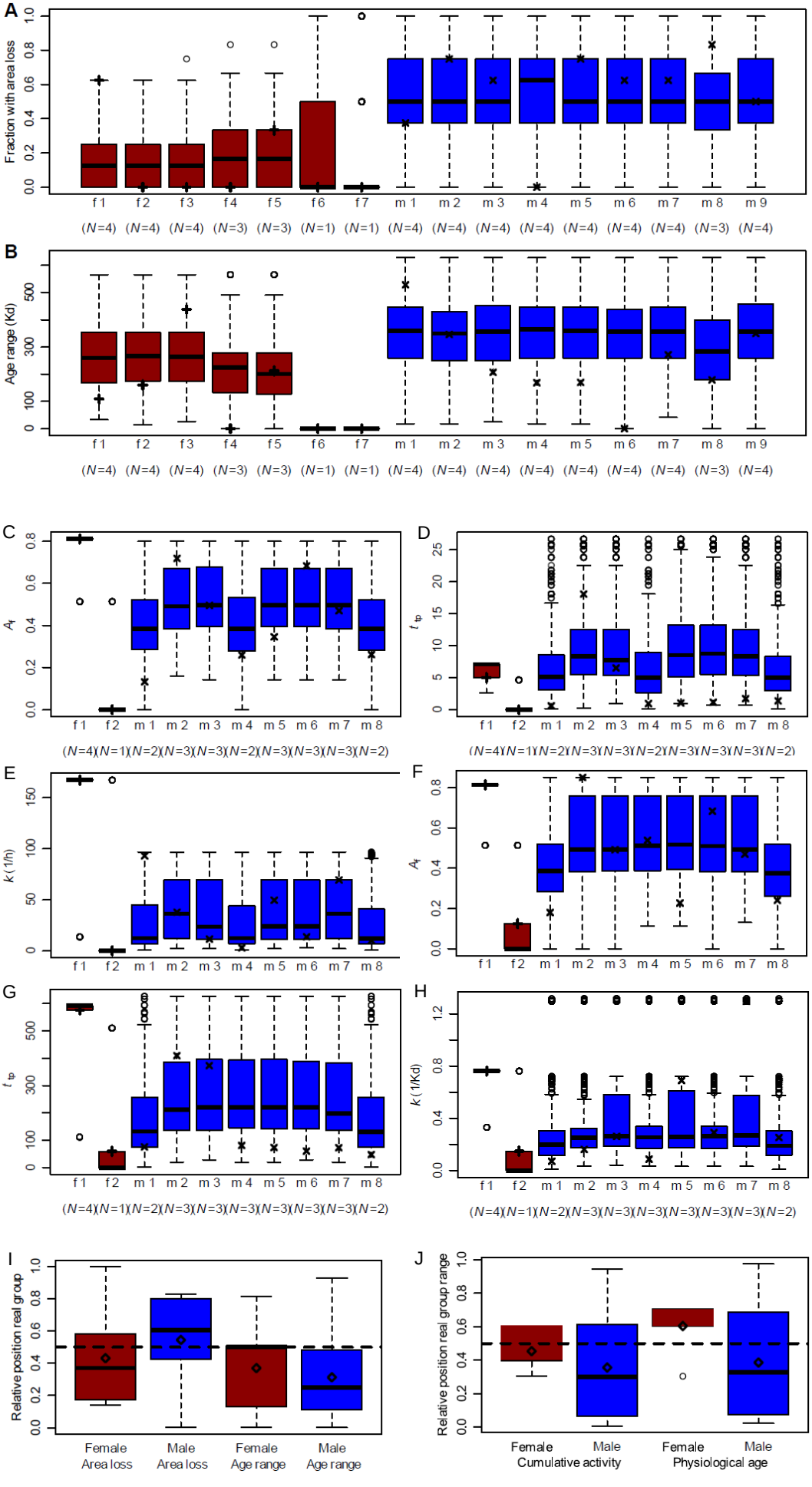
A
Fraction with area loss
f1 f2 f3 f4 f5 f6 f7 m1 m2 m3 m4 m5 m6 m7 m8 m9
(N=4) (N=4) (N=4) (N=3) (N=3) (N=1) (N=1) (N=4) (N=4) (N=4) (N=4) (N=4) (N=4) (N=4) (N=3) (N=4)
B
Age range (Kd)
f1 f2 f3 f4 f5 f6 f7 m1 m2 m3 m4 m5 m6 m7 m8 m9
(N=4) (N=4) (N=4) (N=3) (N=3) (N=1) (N=1) (N=4) (N=4) (N=4) (N=4) (N=4) (N=4) (N=4) (N=3) (N=4)
C
A_f
f1 f2 m1 m2 m3 m4 m5 m6 m7 m8
(N=4)(N=1)(N=2)(N=3)(N=3)(N=2)(N=3)(N=3)(N=3)(N=2)
D
t_{tp}
f1 f2 m1 m2 m3 m4 m5 m6 m7 m8
(N=4)(N=1)(N=2)(N=3)(N=3)(N=2)(N=3)(N=3)(N=3)(N=2)
E
k (1/h)
f1 f2 m1 m2 m3 m4 m5 m6 m7 m8
F
A_f
f1 f2 m1 m2 m3 m4 m5 m6 m7 m8
G
t_{tp}
f1 f2 m1 m2 m3 m4 m5 m6 m7 m8
(N=4)(N=1)(N=2)(N=3)(N=3)(N=3)(N=3)(N=3)(N=3)(N=2)
H
k (1/Kd)
f1 f2 m1 m2 m3 m4 m5 m6 m7 m8
(N=4)(N=1)(N=2)(N=3)(N=3)(N=3)(N=3)(N=3)(N=3)(N=2)
I
Relative position real group
Female Area loss
Male Area loss
Female Age range
Male Age range
J
Relative position real group range
Female Cumulative activity
Male Cumulative activity
Female Physiological age
Male Physiological age

Fig. S5. (A) Relative fraction of wings with wing damage above 15% A_0 loss. (B) Data range (box plot) of physiological age reached by the flies for all permutations (original and permutated groups). Corresponding groups are named "f/m *x*" and correspond to real groups Mf/m*X*, with the number of analysed flies shown below. Circles are outliers and crosses show data range of original group. Red (f) , female groups; blue (m), male groups. (C-E) Cumulative activity of all permutations (original and permutated groups) depicted as box plots. Data range of final relative wing area in *C*, data range of flight activity at the inflexion point of logistic fit in *D*, and data range of logistic growth rate in *E*. Circles are outliers and crosses give the range of the original group (upright for females, tilted for males). (F-H) Data range of physiological age of all permutations (original and artificial groups) depicted as box plots. Data ranges of final relative wing area in *F*, activity at inflexion point of logistic fit in *G*, and logistic growth rate in *H*. (I) Relative rank of fraction of damaged wings and age range of original group compared to all permutations. Data were pooled with respect to group identity. Dashed line at 0.5 indicates no effect of fly group membership. Diamonds, arithmetic means. (J) Relative rank of pooled parameters of successful logistic fits according to cumulative flight activity and physiological age of original group compared with all permutations. Dashed line at 0.5 indicates no effect of fly group membership. Diamonds are arithmetic means.

References

Barthelme, S. (2020). *imager: image processing library based on 'CImg'*. R package version 0.42.3

Chang, W. (2014). *extrafont: Tools for using fonts*. R package version 0.17

Dowle, M. and Srinivasan, A. (2019). *data.table: Extension of 'data.frame'*. R package version 1.12.8

Dunnington, D. and Harvey, P. (2019). *exifr: EXIF image data in R*. R package version 0.3.1

Ellington, C. P. (1984a). The aerodynamics of hovering insect flight. I. The quasi-steady analysis. *Phil. Trans. R. Soc.* B 305(1122), 1–15. doi:10. 1098/rstb.1984.0049

Ellington, C. P. (1984b). The aerodynamics of hovering insect flight. II. Morphological parameters. *Phil. Trans. R. Soc.* B 305(1122), 17–40. doi: 10.1098/rstb.1984.0050

Elzhov, T. V., Mullen, K. M., Spiess, A.-N. and Bolker, B. (2016). *minpack.lm: R Interface to the Levenberg-Marquardt Nonlinear Least-Squares Algorithm Found in MINPACK, Plus Support for Bounds*. R package version 1.2-1

Gagolewski, M. (2020). *R package stringi: Character string processing facilities*

Keitt, T. (2012). *colorRamps: Builds color tables*. R package version 2.3

Komárek, A., Lesaffre, E. and Hilton, J. F. (2005). Accelerated failure time model for arbitrarily censored data with smoothed error distribution. *J. Comp. Graph. Statistics* 14(3), 726–745. doi:10.1198/106186005x63734

Ligges, U., Krey, S., Mersmann, O. and Schnackenberg, S. (2018). *tuneR: Analysis of Music and Speech*

Lisovich, A. and Day, R. (2014). *rChoiceDialogs: rChoiceDialogs collection*. R package version 1.0.6

Mangiafico, S. (2020). *rcompanion: functions to Support Extension Education Program Evaluation*. R package version 2.3.26

McAlpine, J. F. (1981). *Manual of Nearctic Diptera*. Ottawa: Research Branch, Agriculture Canada. ISBN 0660107317

Ooms, J. (2020). *magick: Advanced Graphics and Image-Processing in R*. R package version 2.4.0

Plate, T. and Heiberger, R. (2016). *abind: combine multidimensional arrays*. R package version 1.4-5

R Core Team (2020). *R: A Language and Environment for Statistical Computing*. R Foundation for Statistical Computing, Vienna, Austria

Sarkar, D. (2008). *Lattice: Multivariate Data Visualization with R*. New York

Schindelin, J., Arganda-Carreras, I., Frise, E., Kaynig, V., Longair, M., Pietzsch, T., Preibisch, S., Rueden, C., Saalfeld, S., Schmid, B. et al. (2012). Fiji: an open-source platform for biological-image an alysis. *Nature Methods* 9(7), 676–682. doi:10.1038/nmeth.2019

Skovgård, H. and Nachman, G. (2004). Biological control of house flies *Musca domestica* and stable flies *Stomoxys calcitrans* (Diptera: Muscidae) by means of inundative releases of *Spalangia cameroni* (Hymenoptera: Pteromalidae). *Bulletin of Entomoll Res.* 94(6), 555–567. doi: 10.1079/ber2004322

Urbanek, S. (2013a). *png: Read and write PNG images*. R package version 0.1-7

Urbanek, S. (2013b). *tiff: Read and write TIFF images*. R package version 0.1-5

Urbanek, S. (2019). *jpeg: Read and write JPEG images*. R package version 0.1-8.1

Weis-Fogh, T. (1973). Quick estimates of flight fitness in hovering animals, including novel mechanisms for lift production. *J. Exp. Biol.* 59, 169–230